Reply to comments from referee 1 “Interactive comment on “231Pa and 230Th in the ocean model of the Community Earth System Model (CESM1.3)” by Sifan Gu and Zhengyu Liu”

We thank the reviewer for his/her time for constructing the comments.

In the following, we have addressed all comments, with the original review text underlined in italics and red.

Comments: 1) The authors seem unaware of the recent paper by Rempfer et al (2017, EPSL) which describes in detail how Pa and Th are implemented in their 3D ocean model. Their description is more comprehensive and complete in the sense that an interested reader has all information available to carry out the model development in another model. This comprehensiveness is also a hallmark of the earlier paper by Siddall et al (2005, EPSL). The paper here, however, does not provide the detail this reviewer is expecting of a GSMD contribution. The paper needs to take the Rempfer study into consideration and describe carefully in which way the authors' approach is the same, or where it deviates, and why. In the latter case, all parameter values are to be given, as this is a contribution to GSMD (with emphasis on Development which means that a developer can take this paper and create a Pa, Th model component from this information). A the current stage, the paper does not provide this information.

Thanks for pointing out the paper by Rempfer et al., (2017). We have made substantial changes describing how Pa and Th are implemented in our model and the difference between Rempfer et al., (2017). We add a short review on previous modeling efforts (Line 80-89) and the similarity and difference between our method and previous studies (Line 200-207). Eq. (3) is the conservation equation for Pa and Th, which is how Pa and Th calculated in the model. The calculations of Pa and Th are based on this equation. In section 2.3, we explicitly describe each term in Eq. (3) and the values of different parameters, which includes all the information for reproduce the model development in another model. Also, we add Table 1 and Table 2 to show the abbreviation and values of different parameters used in text.

2) Comment 1) does not only apply to the model description only but also to the one example Gu and Liu show, the effect of a collapse of the AMOC on Pa and Th. Rempfer et al (2017) carried out a water hosing experiment and analysed in detail how changes in the Pa/Th ratio inform about circulation changes in the North Atlantic. A critical comparison of the present results with Rempfer et al. is missing.

In the revised version, we compare our results with Rempfer et al. 2017. We get similar particulate Pa/Th response in North Atlantic (their Fig. 8 and our Fig. 12) and we add a discussion in the text (Line 423-444).

3) The authors state on line 134 that their implementation is based on Siddall et al (2005). Does this mean that it is identical, i.e. all the parameter values are the same? If not, a Table with the parameter values would be needed for complete information. As *stated above, this would be a requirement fro GSMD; too many studies are published nowadays with incomplete information.*

Sorry we did not make this clear enough. Yes, the parameters in the implementation is the same as Siddall et al., (2005). Values of different parameters are given in the text when it first appears. To make it clearer, we add a table to summarize the parameters and variable in Table 1 and Table 2.

4) The text on lines 144ff does some forward referencing to the equations. This should be avoided. First set the context, then introduce the equations and describe every parameter and variable that occurs in these equations. This would ensure easier reading. For example, eq 4 shows many parameters whose values are not given. On line 167 the authors say that eq 4 can be derived from (1) and (2). This is not obvious from the formulations of (1) and (2). Rather eq 4 is a variant of eq 10 of Siddall et al (2005). Again more detail and clarity are needed here.

Thanks for pointing out the problems in the equations. We have rearranged the context and the equations as suggested. We explicitly show how A_p^i can be calculated from Eq. 1 and 2 (Eq. 4, 5 and 6).

5) A central point of this paper is the implementation of Pa and Th in abiotic and biotic formulations. In order to appreciate this, more description and analysis should be provided. For example, the prescribed and simulated particle fluxes in different ocean provinces should be shown and compared. It should be quantified how and where they differ in order to better understand the consequence of these choices for Pa and Th. Given the present level of information in the paper, one can be convinced that the agreement of the two approaches for the control simulation is satisfactory. However, in the transient experiments, differences are rather large depending on the location where the variations are analysed (Fig. 7). Without a more detailed description, the reader is unable to understand the differences. For example, it would be most useful in Fig. 2 below the first row to add panels of the biotic simulation for direct comparison. Implicitly, this information is provided in the scatter plots e)-h), but it would be easier for the reader to see the spatial distribution for the concentrations of the four constituents next to one another and to compare abiotic with biotic this way.

First of all, the term abiotic and biotic seems to be not appropriate since Pa and Th are not actually involved in the biological activity. We change the term to “p-fixed” and “p-coupled” which clearly indicates the difference between two versions.

Thanks for suggesting ways to show that the p-fixed and p-coupled versions give almost identical results in CTRL. We follow this advice and show directly the results of these two versions in Fig. 2, 3 and 4. Clearly, readers can see that p-fixed and p-coupled are similar in CTRL.

For the HOSING experiment, we also add Fig. 8 to show the differences in particle production during AMOC_on and AMOC_off, which will help the discussion about the p-fixed and p-coupled Pa/Th differences in HOSING.

8) The authors follow the approach of Siddall et al (2015) and Rempfer et al (2017) to compare their control simulation with observations. Information is incomplete here as to which data has been used for this comparison. A table in the paper or in the supplementary material summarizing which data has been used would be helpful.
Thanks for suggesting to use a table to show the data used. We have added Table 3 to show the references used in model data comparison. Most of the data are also used in Rempfer et al., (2017).

9) Further to 8) reference to the important effort of GEOTRACES is missing. GEOTRACES offers a wealth of relevant new data. They were used in Rempfer et al (2017) and should also be incorporated into this study for a better and more comprehensive comparison.
Thanks for pointing out available GEOTRACES data. We have included those in the observation (Table 3). We show model results along two GEOTRACES transects as in Rempfer et al., (2017) (Fig. 2 and 3) for direct comparision. Our results are similar as the case Re3d in Rempfer et al. (2017), which does not include boundary scavenging and sediment resuspensions.

10) Information is missing under what conditions Exp_1 and Exp_2 were run. Were these abiotic or biotic simulations? Also, this is not evident in Fig. 5.
Sensitivity experiment Exp 1 and Exp 2 are abiotic simulations for computational efficiency (Line 212-213). Exp1 and Exp2 are carried under the same forcing as CTRL (Line 221-222).

11) In Fig. 2b high values of Th_d are noted in the Southern Ocean. This is in contrast to Siddall et al. (2005, their Fig.2) and should be discussed. Is this also occurring in the biotic simulations (see also comment 7. Might the opal fluxes be too high there?
Since the GEOTRACE transects are more appropriate for model data comparison, we replace the zonal mean figure with the GEOTRACE transects and move the zonal mean figure to the supplementary information (Fig. S3). The high values of Th_d in the Southern Ocean around 60°S in the model is consistent observations (Fig. S3b) since observations of Th_d from 60°S-55°S are much larger than Th_d from 55°S-40°S. In addition, our model is in much higher resolution than Siddall et al., (2005). The maximum Th_d locates at around 60°S, decreasing if further southward in our model. Similar pattern also appears in Siddall et al., (2005). Their Th_d maximum is at around 55°S, decreasing southward (but only two grid available in their model).

12) Lines 237-240: This statement is not instructive, nor is it very useful. It is noted that the author have performed only one quite simple sensitivity experiment, and this is increasing or decreasing K which changes all partition coefficients simultaneously. This limited perspective does, of course, not shed too much light on this important question. At least some more thoughts by the authors should be offered here, if not some more pertinent sensitivity tests with their model.
Thanks for pointing this out. We have removed this part. The poor performance in simulating particulate Pa and Th is also in Siddall et al., (2005) and Dutay et al., (2009). Rempfer et al., (2017) only shows Pa_p/Th_p and does not show individual Pa_p and

Th_p. It's possible the performace is limited by our choice of modeling scheme since the process in controlling Pa and Th activities are essentially the same among our study, Siddall et al., (2005) and Dutay et al., (2009). Although individual Pa_p and Th_p do not agree well with the observations, the ratio of Pa_p/Th_p in our CTRL experiment show similar results as in Rempfer et al. (2017) and sediment Pa_p/Th_p distribution agrees with available observations. And the ratio of Pa/Th is what we are interested in.

13) Section 4.3. Here, a deeper analysis is required, in particular a comparison with the recent paper of Rempfer et al (2017). They provide an interesting spatial consideration of correlation and Pa/Th-AMOC sensitivity in the North Atlantic Ocean in order to shed light on the controversy whether, and to what extent, Pa/Th changes reflect AMOC changes. The paper here would be able to make an important further contribution to this question, but this opportunity is missed. The authors may argue that this is a paper for GSMD, and hence addressing scientific questions is not the primary purpose. This reviewer might agree with this view if the necessary information for model developers. At this stage, unfortunately, neither is the case.

Thanks for pointing out the interesting spatial dependence behavior of Pa/Th in the hosing experiment in Rempfer et al., 2017. Our model, with much higher resolution, shows similar spatial pattern as theirs (Fig. 12). We add discussion of this spatial dependence in Line 423-444. This spatial dependence is mainly caused by AMOC, since the pattern in p-fixed and p-coupled are similar.

14) On line 307 the authors argue that the abiotic version captures the major features of the transient simulation. Considering Fig. 7c, d, e, f this statement seems overstating the agreement. Important differences in the transient signal are evident. This should be discussed and explained.

We agree that there are many differences between p-fixed and p-coupled response to freshwater forcing. If we compare Fig. 10 b and d, in North Atlantic, the sediment Pa/Th overall show increase in both p-fixed and p-coupled (except opal maximum region). In Fig. 9, the transient evolution figure, if we neglect the initial drop in p-coupled (red), the long-term trend between p-coupled and p-fixed are the same. Therefore, over low productivity and long time scale, the p-fixed capture the major features of sediment Pa/Th change and suggest that AMOC change is dominant. But on short time scale and over high productivity region, p-coupled response behaves quite differently from p-fixed. We discuss the differences in the revised manuscript (Line 381-420).

15) From Table 1 it is evident that dust input was not considered in these experiments, although this is not explicitly stated in the text. It would be important to inform the reader why this choice was made, or better, quantify the effect on the Pa and Th concentrations if dust input is included in the simulations.

Thanks for the suggestions. Dust is not included in the calculation. We use the parameters used in the control experiment in Siddall et al., (2005), which the partition coefficient for dust is 0. They also did sensitivity experiment and find dust flux is unimportant for Pa/Th fractionation. We have modified Fig.1, Table 1 and text (line135-137) accordingly.

16) line 383-385. The authors seemed to copy this part from another of their GSMD papers.

Sorry for the mistake in the code availability part. We have fixed the error.

17) Throughout the paper, the English should be carefully revisited, in particular in section 4.3. In that section, more paragraphs would ease the reading.

Follow this suggestion, we re-write section 4.3. In the revised version, we first discuss the p-fixed sediment Pa/Th response in the Atlantic, which generally increase during AMOC_off (Line 339-358) and the magnitude of increase is related to particle distribution (Line 359-370). Then we discuss the p-coupled response. The change in sediment Pa/Th between AMOC_on and AMOC_off in p-coupled are similar to p-fixed in most North Atlantic (Line 371-380), but there are differences especially on short time scale and over high productivity region (Line 381-420). At last, we discuss the change in particulate Pa/Th in North Atlantic and show the depth dependence of the change (Line 423-444).

Reply to comments from referee 2

We thank the reviewer for his/her time for constructing the comments.

In the following, we have addressed all comments, with the original review text underlined in italics and red.

"The paper 231Pa and 230Th in the ocean model of the community Earth system model (CESM1.3)" by S. Gu and Z. Liu is presenting the implementation of 231Pa and 230Th in their general circulation model. It is mainly following the procedure defined by previous work Siddall et al (2005) and Dutay et al (2009). The implementation of the tracers in the model is described and results are compared to observations. However some severe weaknesses are found in the manuscript. The comparison with observation is insufficient, it is strictly following the analysis performed by Siddall et al in 2009, while It now exists , thanks to the GEOTRACES project, new data set. Moreover, the paper do not only show the implementation of the tracer in the model and its validation, which is the scope of the GMD journal, It also propose the response to hosing experiments that is paleoclimate studies that are application that are not devoted to this journal, Climate of the past would be a more appropriate journal if this study was more correctly analysed. For all these reasons I propose to reject this paper from publication in GMD."

Thanks for pointing out the new data set provide by GEOTRACES. In our revised manuscript, we include this new data set. A recent study by Rempfer et al., (2017) shows ^{231}Pa and ^{230}Th in Bern3D model. We also compare our results with theirs.
The results in the hosing experiment is an example to show the advantages of our model. The interpretation of sediment ^{231}Pa/^{230}Th as a paleo proxy for reconstructing AMOC has been questioned because it will also be influenced by particle flux change. Our model includes two versions of ^{231}Pa and ^{230}Th, which can help to detangle these two effects. The hosing experiment is an example to show that with these two versions of ^{231}Pa and ^{230}Th, our model is able to help the interpretation of paleo ^{231}Pa/^{230}Th reconstructions. GMD encourage submissions with "tangible and potentially useful advance related to model development" (Editorial 1.1, Introduction) and we think the content in the hosing experiment fits this scope.

"Specific comments: Page 4 section 2.2. The authors show particle flux surface horizontal distribution without concrete comparison with observation. This diagnostic is interesting but it is not sufficient for the proposed study. The model uses particle concentrations and results are strongly dependent to the quality of these fields. It now exist observations to validate the particle fields (Lam et al, 2015) that were not available for Siddall et al (2005) and Dutay et al (2009). A more detailed analysis of the vertical particle concentration distribution at large scale is required."

The particle fields used in this study is generated from the ecosystem module of the CESM, which has been validated extensively in previous studies (e.g. Doney et al., 2009; Long et al., 2013; Moore et al., 2002, 2004; Moore and Braucher, 2008). The export production is similar to satellite observations in both pattern and magnitude (Sarmiento and Gruber 2006). Global average POC concentration is $2.6*10^{-6}$ kgC/m^3; $CaCO_3$ is $1.1*10^{-6}$ kgC/m^3 and opal is $3.9*10^{-6}$ kgSi/m^3, consistent with Rempfer et al., (2011). Therefore, the particle fields in CESM is more or less right, although regional discrepancies from observation may exist. We appreciate the reviewer's suggestion to validate the performance of the ecosystem module of the CESM with new data. But our focus of study is the Pa/Th in the model.

Also, we show the distribution of particle fields to help the discussion of sediment $^{231}Pa/^{230}Th$, which is influenced largely by particle distribution. Compare with Siddall et al., 2005, Dutay et al., 2009, and Rempfer et al., 2017, all models use particle fields generate from different models (but the general patterns are the same) but yields similar ^{231}Pa and ^{230}Th results.

"Page 5 section 2.3 Abiotic and Biotic name for simulations are not appropriate. These names suggest that the tracers are subject to different processes while it is not the case. The two approaches are the same except that the particles fields are fixed in the Abiotic run. None biogeochemical process affects the tracer except adsorption and desorption onto particles, so the appellation Biotic run seems exaggerated. Line 162: No validation of particle fields is preformed while it affect strongly the model results. Observations are now available (see for instance lam et al 2015)"

Thanks for pointing out this inappropriate usage. We have renamed the version which is coupled to the ecosystem model as "p-coupled" and the version which uses prescribed particle fields as "p-fixed".

"Pages 7 and 8 section 4, results Definition and way of estimation of the residence time given for the tracers should be explained."

The residence time is calculated as the ratio of global average total isotope activity and the radioactive ingrowth of the isotope. The way of calculated is used in Rempfer et al., (2017) and Yu et al., (1996). We add this in the revised manuscript (line 248-249).

"Comparison of Atlantic zonal averaged model results with observations is no more adequate. It is strictly following analysis performed by Siddall et al (2005) and Dutay et al (2009) a decade ago, but now many new observations are available in the different basins thanks to the GEOTRACES program. This validation is not appropriate any more. Discussion concerning the ratio 231Pa/230Th is very poor. More detailed analysis must be given. For instance what causes low ratio in the north atlantics south of Grennland: convection?"

With the new GEOTRACES data, we update the model data comparison with two GEOTRACES transects in the Atlantic (Fig.2 and 3). This is a more appropriate comparison than Atlantic zonal mean figure.

The large-scale feature of sediment $^{231}Pa/^{230}Th$ is small value in North Atlantic and large value in the Southern Ocean discussed in line 282-293. Regionally, the distribution of sediment $^{231}Pa/^{230}Th$ is controlled by particle distribution (especially opal) due to the particle flux effect (line 56-58). The low values south of Greenland at about 50°N is because of this particle flux effect (line 293-296). Opal production is larger in both south and north of this region. Therefore, the particle flux effect will transport 231Pa out of this region, resulting lower sediment $^{231}Pa/^{230}Th$ in this region and higher sediment $^{231}Pa/^{230}Th$ north and south of this region.

"Page10 and 11. This part is already an attempt to use the model development for scientific question. It is not the purpose of GMD papers. This part should be more deeply analysed and submitted to another more appropriate journal (eg climate of the past)"

The purpose of implementing ^{231}Pa and ^{230}Th in CESM is to provide a tool to better interpret sediment $^{231}Pa/^{230}Th$ reconstructions. The advance of our modelling study compared with previous studies is that we have two version of ^{231}Pa and ^{230}Th to separate the circulation effect and particle effect, both of which will change in response to freshwater forcing. Section 4.3 is to examine this model feature and show that although circulation effect dominates sediment $^{231}Pa/^{230Th}$ over low productivity regions in the North Atlantic and on long time scale, particle effect can be important over high productivity region and on short time scale. This part is an example to show the model advantage to detangle these two effects and therefore we think it is important to include this part to demonstrate our model advantage.

Reply to comments from referee 3

We thank the reviewer for his/her time for constructing the comments.

In the following, we have addressed all comments, with the original review text underlined in italics and red.

"The main point of criticism I have here is their comparison to observational data, which I find is too nebulous and not supported by newer data. There is an obvious lack of consideration of recent papers. More recent studies would provide a much better basis for comparison and reality-checks of the model. The references for the observational data given in the MS are quite old holding mostly data obtained by the noisy counting-method resulting in large analytical uncertainties. Instead the model should be cross-checked with newer sedimentary and water column data. I don't see much benefit from comparing "biotic" against "abiotic" 231Pa and 230Th particle-fluxes (Fig. 2), as long as the absolute values have not been tested against new observational data. The authors urgently need to test the output of the model versus recent sedimentary data (e.g. (Böhm et al., 2015; Bradtmiller et al., 2014; Burckel et al., 2016; Henry et al., 2016; Hoffmann et al., 2013; Jonkers et al., 2015; Lippold et al., 2011; Lippold et al., 2016; Lippold et al., 2012; Luo et al., 2015; Negre et al., 2010; Roberts et al., 2014; Rutgers van der Loeff et al., 2016)), water data (e.g. (Deng et al., 2014; Hayes et al., 2014; Hayes et al., 2013; Hayes et al., 2015a; Hayes et al., 2015b; Kretschmer et al., 2011)) and most importantly other modelling studies (e.g. (Dutay et al., 2015; Lippold et al., 2011; Rempfer et al., 2017))."

Thanks for pointing recent available observations. We have updated our analysis with more complete data. The references for observations are listed in Table 3, which includes all the references used for model data comparison in Rempfer et al., (2017). Unfortunately, there is no intercalibrated dataset available.

In the revised manuscript, we replace the zonal mean figure with the GEOTRACE transects (Fig. 2 and 3), which seems to be more appropriate for direct model-data comparison. These two GEOTRACES transects are also shown in Rempfer et al. 2017. Our modelling scheme is essentially the same as Siddall et al., (2005) and the experiment Re3d in Rempfer et al., (2017), which does not include boundary scavenging and sediment resuspensions. Our results along the two GEOTRACES transects are similar to the Re3d in Rempfer et al., (2017). For dissolved ^{231}Pa and ^{230}Th, our model can simulate the right magnitude as in observations (Fig. 2 and 3) except in the abyssal. The larger values in the abyssal compared with observations is because we do not include boundary scavenging and sediment resuspensions in our model. As shown in Rempfer et al., (2017), if boundary scavenging and sediment resuspensions are added, the model performance in simulating the dissolved ^{231}Pa and ^{230}Th will be much improved (their Fig. 2 and 3 top and bottom row). This is discussed in the revised manuscript (Line 255-263).

Rempfer et al., (2017) suggests that boundary scavenging and sediment resuspensions are unimportant for particulate $^{231}Pa/^{230}Th$. Our particulate $^{231}Pa/^{230}Th$ (Fig. 2c and Fig. 3c) in the Atlantic show similar results as Rempfer et al., (2017). Most importantly, our sediment $^{231}Pa/^{230}Th$ compares well with available observations (Fig. 4): low values in North Atlantic and high values in the Southern Ocean; high values in high productivity regions (Line 281-296).
In addition, we show side by side comparison between "abiotic" and "biotic" version in revised Fig. 2, 3 and 4 to directly show that the two versions give identical results in CTRL (Line 237-246). Although these two are similar in CTRL, they do vary differently in the HOSING experiment. Therefore, we find it may be clearer for readers to directly see the comparison between the two version in both CTRL and HOSING.

"I find the terms "biotic 231Pa/230Th" and "abiotic 231Pa/230Th" quite confusing. Since there is no biotic 231Pa and 230Th these terms should be used only to distinguish between the usage of particle fields in the model."

Thanks for pointing out this inappropriate usage. We have renamed the version which is coupled to the ecosystem model as "p-coupled" and the version which uses prescribed particle fields as "p-fixed" as suggested.

"Given that (Rempfer et al., 2017) recently provided insights into an upgraded approach by (Siddall et al., 2005) and (Siddall et al., 2007), including a bio-geochemical-module in the model, I do not see much advance provided by the here presented MS. I did not find a reference to (Rempfer et al., 2017), maybe because this is a very recent publication, but I don't think the authors should neglect this paper in a new version."

Thanks for referring to Rempfer et al., (2017). We add comparison with their results in the revised manuscript. In CTRL, our water column dissolved ^{231}Pa and ^{230}Th is similar as Re3d in Rempfer et al., (2017) which do not include boundary scavenging and sediment resuspensions. The particulate $^{231}Pa/^{230}Th$ in the Atlantic is also similar to Rempfer et al., (2017). In the hosing experiment, our model produces the similar spatial dependence of particulate $^{231}Pa/^{230}Th$ in the Atlantic (our Fig. 12 and their Fig.8). The text referring to Rempfer et al., 2017 are in line 86-89, 202-207, 255-263, 423-444.

"Although I welcome very much the provision of the Fortran code the reader is left alone with the comparison between model and observations (Fig.3) without sufficient information about the values, observational error bars and references. The color code in Fig. 3 may hold some information about the water depths, but since (already) older publications demandingly have shown, that the correlation of 231Pa/230Th with water-depth seems to be a manifested pattern of AMOC in the 231Pa/230Th distribution (Burckel et al., 2016; Gherardi et al., 2009; Gherardi et al., 2010; Hoffmann et al., 2013; Luo et al., 2010; Luo et al., 2015) this feature is required to be reproduced by a meaningful model. But I'm not able to see this from the provided figures."

Thanks for pointing out the important depth dependence of $^{231}Pa/^{230}Th$. In our revised Fig. 2 and 3, particulate $^{231}Pa/^{230}Th$ in the Atlantic transects are shown. $^{231}Pa/^{230}Th$ increases with depth as suggested by previous studies (Line 277-280). We also show North Atlantic average particulate $^{231}Pa/^{230}Th$ profile in Fig.12. We further discuss this depth dependence in the HOSING experiment (Line 423-444). Our results supports the argument that this depth dependence is caused by the lateral transport of ^{231}Pa by ocean circulation (Gherardi et al., 2009; Lippold et al., 2011, 2012; Luo et al., 2010).

"By the way, the diagrams are way too detailed (in terms of graphic resolution) demanding a lot of computer resources and slowing down even my reasonably new computer just by scrolling down."

Sorry the resolution of figure is too large. We have compress this figure in the revised manuscript.

"The table for the K values (Table 1) needs to be accompanied by references, because these values vary within a wide range according to the studies by (Chase et al., 2002, 2004; Hayes et al., 2013; Hayes et al., 2015b; Kretschmer et al., 2011; Kretschmer et al., 2008; Luo et al., 1999, 2003, 2004) and others. I think, a well selected digest of values can be found at the new study by (Rempfer et al., 2017)."

The K values used in our control experiment are the same as what used in Siddall et al., (2005), which is from Chase et al., (2002). We have added these references in the Table 2 (originally Table 1) caption in the revised manuscript.

"Besides the shortcomings of the MS regarding the observational data, I also find patterns in the model output, which are not observed in reality to my knowledge. E.g. the appearance of a high opal/POC field in the NW-Atlantic. Further, I see an obvious mismatch of model and observations in Fig. 5, which is not explained."

The particle fields are produced by the marine ecosystem module in CESM. This ecosystem module is have been discussed in many previous studies (e.g. Doney et al., 2009; Long et al., 2013; Moore et al., 2002, 2004; Moore and Braucher, 2008) (Line 122-123). The general pattern globally is similar to the satellite observations (Sarmiento and Gruber 2006). For example, low production in subtropical gyre; high opal in the Southern Ocean. Regionally, the mismatch can be caused by many different aspects, such as modelling scheme, model resolution and biases in boundary conditions. How to improve the performance of the marine ecosystem module is beyond the scope this study.

The Fig. 6 (originally Fig. 5) shows the results of sensitivity experiments. The discussion is in line 303-310. The mismatch of model and observation is reasonable since we change the partition coefficients K in these two experiments. Take EXP_1 for example, the simulated dissolved ^{231}Pa and ^{230}Th (Fig. 6 and b) are much larger than observations because in EXP_1, K is decreased from CTRL by a factor of 5. Smaller K means smaller sink for ^{231}Pa and ^{230}Th, with the source kept the same, dissolved ^{231}Pa and ^{230}Th will increase. The mismatch of model and observations also suggest that K is in the correct magnitude in CTRL.

"In summary, it is hard for me to see that the here presented model approach provides any new insights on the 231Pa/230Th method. Due to the lack of information about the model-data comparison it is not possible to assess the quality of the model and the applied parameters. Consequently I suggest revising both the model runs and the MS thoroughly before publication can be considered."

In our revised manuscript, we compare our model results with new GEOTRACES data and also compare with the recent modelling study by Rempfer et al., (2017). Overall, our model can simulate the general features in water column ^{231}Pa and ^{230}Th and sediment ^{231}Pa/^{230}Th. Different from Rempfer et al., (2017), we have two versions of ^{231}Pa and ^{230}Th: p-fixed and p-coupled, which have the advantage to detangle the circulation effect and particle effect in controlling sediment ^{231}Pa/^{230}Th. In our hosing experiment, these two version of ^{231}Pa and ^{230}Th do show different responses. Therefore, our model is a useful tool to improve the interpretations of ^{231}Pa/^{230}Th reconstructions.

^{231}Pa and ^{230}Th in the ocean model of the Community Earth System Model (CESM1.3)

Sifan Gu[1], Zhengyu Liu[1,2]

[1]Department of Atmospheric and Oceanic Sciences and Center for Climate Research, University of Wisconsin-Madison, Madison, WI, USA

2. Now, affiliated with: Atmospheric Science Program, Department of Geography, Ohio State University

Correspondence to: Sifan Gu (sgu28@wisc.edu)

Abstract

Sediment ^{231}Pa/^{230}Th activity ratio is emerging as an important proxy for deep ocean circulation in the past. In order to allow for a direct model-data comparison and to improve our understanding of sediment ^{231}Pa/^{230}Th activity ratio, we implement ^{231}Pa and ^{230}Th in the ocean component of the Community Earth System Model (CESM). In addition to the p-coupled ^{231}Pa and ^{230}Th that is fully coupled with the active marine ecosystem module, another form of p-fixed ^{231}Pa and ^{230}Th have also been implemented with prescribed particle flux fields of the present climate. The comparison of the two forms of ^{231}Pa and ^{230}Th helps to isolate the influence of the particle fluxes from that of circulation. Under present day climate forcing, our model is able to simulate water column ^{231}Pa and ^{230}Th activity and sediment ^{231}Pa/^{230}Th activity ratio in good agreement with available observations. In addition, the p-coupled and p-fixed sediment ^{231}Pa/^{230}Th activity ratios behave similarly over large areas of low productivity on long timescale to freshwater forcing, but can differ substantially in some regions of high productivity and on short timescale, indicating the importance of biological productivity in addition to physical circulation. Therefore, our model provides a potentially powerful tool to help our interpretation of sediment ^{231}Pa/^{230}Th reconstructions and to improve our understanding of past ocean circulation and climate changes.

Deleted:

Deleted: abiotic

Deleted: For past climate, our model is able to simulate a comparable magnitude of the change of sediment ^{231}Pa/^{230}Th activity ratio between the state with and without active AMOC in reconstruction.

Deleted: in hosing experiments,

Deleted: biotic

Deleted: abiotic

1. Introduction

Sediment ^{231}Pa/^{230}Th activity ratio has been used as a proxy to reconstruct ocean circulation in the past (e.g. Yu et al. 1996; McManus et al. 2004; Gherardi et al. 2009). ^{231}Pa (32.5 ka half-life) and ^{230}Th (75.2 ka half-life) are produced at a constant rate approximately uniformly in the ocean by the α decay of ^{235}U and ^{234}U, respectively, with a production activity ratio of 0.093 (Henderson and Anderson, 2003). Water column ^{231}Pa and ^{230}Th are subject to particle scavenging and transport to sediments (Bacon and Anderson, 1982; Nozaki et al., 1987). Differential scavenging efficiency results in different ocean residence time: ^{231}Pa has a residence time of approximately 111 years and ^{230}Th has a residence time of approximately 26 years (Yu et al., 1996). Longer residence time of ^{231}Pa than ^{230}Th makes ^{231}Pa more subject to ocean transport and therefore in modern ocean about 45% of ^{231}Pa produced in the Atlantic is transported to the Southern Ocean (Yu et al., 1996), resulting a lower than 0.093 sediment ^{231}Pa/^{230}Th activity ratio in the North Atlantic and higher than 0.093 sediment ^{231}Pa/^{230}Th activity ratio in the Southern Ocean.

The application of the principle above to interpret sediment ^{231}Pa/^{230}Th as the strength of Atlantic Meridional Overturning Circulation (AMOC), however, can be complicated by other factors, leading to uncertainties in using ^{231}Pa/^{230}Th as a proxy for paleocirculation (Keigwin and Boyle, 2008; Lippold et al., 2009; Scholten et al., 2008). In addition to ocean transport, sediment ^{231}Pa/^{230}Th is also influenced by particle flux and composition (Chase et al., 2002; Geibert and Usbeck, 2004; Scholten et al., 2008; Siddall et al., 2007; Walter et al., 1997). The region of a higher particle flux tends to have a higher ^{231}Pa/^{230}Th (Kumar et al., 1993; Yong Lao et al., 1992), which is referred to as the "particle flux effect" (Siddall et al., 2005). High particle flux in the water column in a region will favor the removal of isotopes into the sediment, which leads to more isotopes transported into this region due to the down-gradient diffusive flux into this region and subsequently more removal of isotopes into the sediment. Since ^{231}Pa has a longer residence time, this effect is

Deleted: o

Deleted: c

Deleted: tracer

more prominent on ^{231}Pa than on ^{230}Th and therefore sediment ^{231}Pa/^{230}Th will be higher in high productivity regions. Also, opal is able to scavenge ^{231}Pa much more effectively than ^{230}Th, leading to higher ^{231}Pa/^{230}Th in high opal flux regions such as the Southern Ocean (Chase et al., 2002). Moreover, sediment ^{231}Pa/^{230}Th is suggested to record circulation change only within 1000 m above the sediment, instead of the whole water column, complicating the interpretation of sediment ^{231}Pa/^{230}Th reconstructions (Thomas et al., 2006). For example, sediment ^{231}Pa/^{230}Th approaching 0.093 during Heinrich Stadial event 1(HS1) from the subtropical North Atlantic is interpreted as the collapse of the Atlantic Meridional Overturning Circulation (AMOC) (McManus et al., 2004). If sediment ^{231}Pa/^{230}Th only records deepest water mass, it is possible that during HS1, AMOC shoals, as opposed to fully collapse, yet an increase of deep water imported from the Southern Ocean featuring high ^{231}Pa/$^{230\mathrm{Th}}$ can increase the sediment ^{231}Pa/^{230}Th approaching the production ratio (0.093) (Thomas et al., 2006). All these suggest the importance of incorporating ^{231}Pa and ^{230}Th into climate models for a direct model-data comparison for a thorough understanding of sediment ^{231}Pa/^{230}Th as well as past ocean circulation.

^{231}Pa and ^{230}Th have been simulated in previous modeling studies (Dutay et al., 2009; Luo et al., 2010; Marchal et al., 2000; Rempfer et al., 2017; Siddall et al., 2005). Marchal et al., (2000) simulates ^{231}Pa and ^{230}Th in a zonally averaged circulation model, using the reversible scavenging model of Bacon and Anderson, (1982). One step further, Siddall et al. (2005) extends Marchal et al., (2000) by including particle dissolution with prescribed particle export production in a 3-D circulation model. Rempfer et al., (2017) further couples ^{231}Pa and ^{230}Th with active biogeochemical model and includes boundary scavenging and sediment resuspensions to improve model performance in simulating water column ^{231}Pa and ^{230}Th concentration. Here we follow previous studies to implement ^{231}Pa and ^{230}Th into the Community Earth System Model (CESM). Our model ^{231}Pa and ^{230}Th are coupled with active marine ecosystem model ("p-coupled") and therefore can be used to study the impact of ecosystem change on ^{231}Pa and ^{230}Th directly. To help to understand the influence of the particle flux, we have also implemented a "p-fixed"

Deleted: (Dutay et al., 2009; Henderson et al., 1999; Marchal et al., 2000; Siddall et al., 2005)

Deleted: (

Deleted:)

Deleted: the scheme of Siddall et al., (2005) to

Deleted: Siddall et al., (2005) uses prescribed particle fluxes.

Deleted: to a

Deleted: biotic

Deleted: n abiotic

version of ^{231}Pa and ^{230}Th, for which the particle fluxes are fixed at prescribed values. By comparing the p-fixed ^{231}Pa and ^{230}Th with the p-coupled ^{231}Pa and ^{230}Th, we will be able to separate the effect of circulation change from particle field change. In addition, the p-fixed ^{231}Pa and ^{230}Th can be run without the marine ecosystem module, reducing computational cost by a factor of 3 in the ocean-alone model simulation and therefore making it a computationally efficient tracer for sensitivity studies.

Deleted: abiotic

Deleted: biotic

Deleted: abiotic

This paper describes the details of ^{231}Pa and ^{230}Th in CESM and serves as a reference for future studies using this tracer module. In section 2, we describe the model and the implementation of ^{231}Pa and ^{230}Th. In sections 3, we describe the experimental design. We will finally compare simulated ^{231}Pa and ^{230}Th fields with observations, show model sensitivities on the parameter and also sediment $^{231}Pa/^{230}Th$ ratio response to freshwater forcing in Section 4.

2. Model Description

2.1 Physical Ocean Model

We implement ^{231}Pa and ^{230}Th in the ocean model (Parallel Ocean Program version 2, POP2) (Danabasoglu et al., 2012) of CESM (Hurrell et al., 2013). CESM is a state-of-the-art coupled climate model and studies describing model components and analyzing results can be found in a special collection in Journal of Climate (http://journals.ametsoc.org/topic/ccsm4-cesm1). We run the ocean-alone model, which is coupled to data atmosphere, land, ice and river runoff under the normal year forcing of CORE-II data (Large and Yeager, 2008), using the low-resolution version of POP2 with a nominal 3° horizontal resolution and 60 vertical layers.

2.2 Biogeochemical component (BGC)

CESM has incorporated a marine ecosystem module that simulates biological variables (Moore et al., 2013). The marine ecosystem module has been validated against present day observations extensively (e.g. Doney et al., 2009; Long et al., 2013; Moore et al., 2002, 2004; Moore and Braucher, 2008). The implementation of ^{231}Pa and ^{230}Th requires particle fields: $CaCO_3$, opal and particulate organic carbon

Deleted: POP2

Formatted: Indent: First line: 0.5"

Deleted: four

Deleted: ,

(POC). These particle fields can be obtained from the ecosystem driver from the ecosystem module (Jahn et al., 2015). The ecosystem module simulates the particle fluxes in reasonable agreement with the present day observations. The pattern and magnitude of the annual mean particle fluxes ($CaCO_3$, opal, POC) leaving the euphotic zone at 105m are similar to the satellite observations (Fig. 7.2.5 and 9.2.2 in Sarmiento and Gruber 2006) (Fig. 1 a~c): particle fluxes are higher in the high productivity regions such as high latitudes and equatorial Pacific; opal flux is high in the Southern Ocean. The remineralization scheme of particle is based on the ballast model of Armstrong et al., (2002). Detailed parameterizations for particle remineralization are documented in Moore et al., (2004) with temperature dependent remineralization length scales for POC and opal. We do not consider dust because it is suggested to be unimportant for ^{231}Pa and ^{230}Th fractionation (Chase et al., 2002; Siddall et al., 2005).

2.3 ^{231}Pa and ^{230}Th implementation

^{231}Pa and ^{230}Th are produced from the α decay of ^{235}U and ^{234}U uniformly everywhere at constant rate β^i ($\beta^{Pa} = 2.33*10^{-3}$ dpm m^{-3} yr^{-1}, $\beta^{Th} = 2.52*10^{-2}$ dpm m^{-3} yr^{-1}). ^{231}Pa and ^{230}Th are also subjective to radioactive decay with the decay constant of λ^i ($\lambda^{Pa} = 2.13*10^{-5}$ yr^{-1}, $\lambda^{Th} = 9.22*10^{-6}$ yr^{-1}).

Another important process contributes to ^{231}Pa and ^{230}Th activity is the reversible scavenging by sinking particles (Bacon and Anderson, 1982), which describes the adsorption of isotopes onto sinking particles and desorption after the dissolution of particles. This process transports ^{231}Pa and ^{230}Th downward and leads to a general increase of ^{231}Pa and ^{230}Th activity with depth. The reversible scavenging considers total isotope activity (A_t^i) as two categories (Eq. (1)): dissolved isotopes (A_d^i) and particulate isotopes (A_p^i) (superscript i refers to ^{231}Pa and ^{230}Th) and A_p^i is the sum of the isotopes associated with different particle types ($A_{j,p}^i$) (subscript j refers to different particle types: $CaCO_3$, opal and POC):

$$A_t^i = A_d^i + A_p^i = A_d^i + \sum_j A_{j,p}^i \qquad (1)$$

Deleted: and dust

Deleted: For ocean-alone experiments, atmospheric dust deposition to the surface ocean is prescribed from Luo et al. (2003) (Fig. 1d).

Formatted: Highlight

Formatted: Highlight

Formatted: Highlight

Deleted: Two forms of ^{231}Pa and ^{230}Th are implemented in POP2: abiotic and biotic. Abiotic ^{231}Pa and ^{230}Th use particle fluxes prescribed as annual mean particle fluxes from the CESM marine ecosystem module under present day climate forcing (Fig.1). Biotic ^{231}Pa and ^{230}Th use particle fluxes computed simultaneously from the marine ecosystem module. Abiotic and biotic ^{231}Pa and ^{230}Th can be turned on at the case build time and the biotic ^{231}Pa and ^{230}Th requires the ecosystem module turned on at the same time. ... [1]

Moved (insertion) [1]

Deleted:

Moved (insertion) [2]

Deleted: =1 and 2

Formatted: Not Superscript/ Subscript

Deleted: , respectively

Deleted: as in

Deleted: Eq. (1)

Dissolved and particulate isotopes are assumed to be in equilibrium, which is a reasonable assumption in the open ocean (Bacon and Anderson, 1982; Henderson et al., 1999; Moore and Hunter, 1985). The ratio between the particulate isotope activity and the dissolved isotope activity is set by a partition coefficient, K (Eq. (2)):

$$K_j^i = \frac{A_{j,p}^i}{A_d^i \cdot R_j} \tag{2}$$

, where R_j is the ratio of particle concentration (C_j) to the density of seawater (1024.5 kg m^{-3}). Subscript j refers to different particle types ($CaCO_3$, opal and POC). Values of partition coefficient K used in our control simulation follows Chase et al., 2002 and Siddall et al., 2005 (Table 2).

Particulate isotopes (A_p^i) will be transported by sinking particles, which is described by $w_S \frac{\partial A_p^i}{\partial z}$, where w_s is sinking velocity. We don't differentiate between slow sinking small particles and rapid sinking large particles as in Dutay et al., (2009) and consider all particles as slowly sinking small particles with sinking velocity of w_s =1000 m yr^{-1} (Arsouze et al., 2009; Dutay et al., 2009; Kriest, 2002) as in Rempfer et al., (2017) and Siddall et al., (2005). Any particulate isotopes (A_p^i) at the ocean bottom layer are removed from the ocean as sediment, which is the sink for the isotope budget. Detailed vertical differentiation scheme to calculate this term in the model is in the supplementary material. The reversible scavenging scheme applied here is the same as the neodymium implementation in POP2 (Gu et al., 2017).

Particle fields used in the reversible scavenging can be either prescribed or simultaneously generated from the marine ecosystem module. Therefore, two forms of ^{231}Pa and ^{230}Th are implemented in POP2: "p-fixed" and "p-coupled". P-fixed ^{231}Pa and ^{230}Th use particle fluxes prescribed as annual mean particle fluxes generated from the marine ecosystem module under present day climate forcing (Fig.1). P-coupled ^{231}Pa and ^{230}Th use particle fluxes computed simultaneously from the

Formatted: Indent: First line: 0"

Deleted: and assumes these two phases are

Moved (insertion) [3]

Formatted: Indent: First line: 0"

Deleted: C

Deleted: ,

Deleted: and dust

Deleted: (term

Deleted: *in Eq.* (3)) by sinking particles with

Deleted: a

Deleted: sinking velocity

Deleted: ,

Deleted: which describes the adsorption of isotopes onto sinking particles and desorption after the dissolution of particles (Detailed vertical differentiation scheme to calculate this term in the model is in the supplementary material).

Moved up [1]: This process transports ^{231}Pa and ^{230}Th downward and leads to a general increase of ^{231}Pa and ^{230}Th activity with depth.

Deleted: sizes

Moved up [2]: The reversible scavenging considers total isotope activity (A_t^i) as two categories: dissolved isotopes (A_d^i) and particulate isotopes (A_p^i) (superscript i=1 and 2 refers to ^{231}Pa and ^{230}Th, respectively) as in Eq. (1) and assumes these two phases are in equilibrium, which is a reasonable assumption in the open ocean (Bacon and Anderson, 1982; Henderson et al., 1999; Moore and Hunter, 1985; Roy-Barman et al., 1996).

Moved up [3]: The ratio between the particulate isotope activity and the dissolved isotope activity is set by a partition coefficient, K (Eq. (2)), where C_j is the ratio of particle concentration to the density of seawater (1024.5 kg m^{-3}). Subscript j refers to different particle types ($CaCO_3$, opal, POC and dust).

marine ecosystem module. P-fixed and p-coupled ^{231}Pa and ^{230}Th can be turned on at the case build time and the p-coupled ^{231}Pa and ^{230}Th requires the ecosystem module to be turned on at the same time.

Therefore, the conservation equation for ^{231}Pa and ^{230}Th activity can be written as

$$\frac{\partial A_t^i}{\partial t} = \beta^i - \lambda^i A_t^i - w_s \frac{\partial A_p^i}{\partial z} + Transport \qquad (3),$$

where the total isotope activity is controlled by decay from U (first term), radioactive decay (second term), reversible scavenging (third term) and physical transport by the ocean model (fourth term, including advection, convection and diffusion). A_p^i can be calculated by combining Eq. (1) and Eq. (2):

$$A_t^i = A_d^i + A_d^i \cdot (K_{POC}^i \cdot R_{POC} + K_{CaCO_3}^i \cdot R_{CaCO_3} + K_{opal}^i \cdot R_{opal})$$

$$= A_d^i \cdot (1 + K_{POC}^i \cdot R_{POC} + K_{CaCO_3}^i \cdot R_{CaCO_3} + K_{opal}^i \cdot R_{opal}), \qquad (4)$$

which leads to

$$A_d^i = \frac{A_t^i}{1 + K_{POC}^i \cdot R_{POC} + K_{CaCO_3}^i \cdot R_{CaCO_3} + K_{opal}^i \cdot R_{opal}}, \qquad (5)$$

put this back to Eq.(1), we get

$$A_p^i = A_t^i \cdot \left(1 - \frac{1}{1 + K_{POC}^i \cdot R_{POC} + K_{CaCO_3}^i \cdot R_{CaCO_3} + K_{opal}^i \cdot R_{opal}}\right) \qquad (6)$$

Comparing with previous studies of modeling ^{231}Pa and ^{230}Th, our p-fixed version is the same as Siddall et al., (2002), except that different prescribed particle fluxes are used. The p-coupled version allows coupling to biogeochemical module, which is similar in Rempfer et al., (2017), but we do not include boundary scavenging and sediment resuspensions as in Rempfer et al., (2017) because boundary scavenging and sediment resuspensions are suggested to be unimportant to influence the relationship between $^{231}Pa_p/^{230}Th_p$ and AMOC strength (Rempfer et al., 2017).

Deleted: $A_t^i = A_d^i + A_p^i$ ... [2]

Formatted: Indent: First line: 0"

Deleted: ... [3]

Deleted: from Eq. (4) below

Deleted: . ... [4]

Deleted: 4

Formatted: Subscript

Formatted: Subscript

3. Experiments

Deleted:

We run a control experiment (CTRL) and two experiments with different partition coefficients to show model sensitivity to partition coefficient. We have both p-fixed and p-coupled ^{231}Pa and ^{230}Th in CTRL, but only p-fixed ^{231}Pa and ^{230}Th in sensitivity experiments. Equilibrium partition coefficients for ^{231}Pa and ^{230}Th vary among different particle types and the magnitude of the partition coefficients for different particle types remains uncertain (Chase et al., 2002; Chase and Robert F, 2004; Luo and Ku, 1999). Since the control experiment in Siddall et al., (2005) is able to simulate major features of ^{231}Pa and ^{230}Th distributions, we use the partition coefficients from the control experiment in Siddall et al., (2005) in our CTRL (Table 2). Two sensitivity experiments are performed with decreased (EXP_1) and increased (EXP_2) partition coefficients by a factor of 5 (Table 2).

Deleted: abiotic
Deleted: biotic
Deleted: show abiotic
Deleted: 1
Deleted: 1

All the experiments are ocean-alone experiments with the normal year forcing by CORE-II data (Large and Yeager, 2008). The ^{231}Pa and ^{230}Th activities are initiated from 0 in CTRL and are integrated for 2,000 model years until equilibrium is reached. EXP_1 and EXP_2 are initiated from 1,400 model year in CTRL and are integrated for another 800 model years to reach equilibrium.

Deleted: of

Since sediment $^{231}Pa/^{230}Th$ in North Atlantic has been used to reflect the strength of AMOC, to test how sediment $^{231}Pa/^{230}Th$ in our model responds to the change of AMOC, we carried out a fresh water perturbation experiment (HOSING) with both p-fixed and p-coupled ^{231}Pa and ^{230}Th. Starting from 2,000 model year of CTRL, a freshwater flux of 1 Sv is imposed over the North Atlantic region of 50°N~70°N and the experiment is integrated for 1400 model years until both p-fixed and p-coupled sediment $^{231}Pa/^{230}Th$ ratio have reached quasi-equilibrium. The partition coefficients used in HOSING are the same as in CTRL.

Deleted: T
Deleted: ratio
Deleted: abiotic
Deleted: biotic
Deleted: abiotic
Deleted: biotic

4. Results

4.1 Control Experiment

P-fixed and p-coupled version of ^{231}Pa and ^{230}Th in CTRL show identical results (Fig. 2-4). P-fixed and p-coupled dissolved and particulate ^{231}Pa and ^{230}Th in CTRL are highly correlated with each other with correlations larger than 0.995 and

Deleted: Abiotic
Deleted: biotic
Deleted: Abiotic
Deleted: biotic
Deleted: (Fig. 2e-h)

regression coefficients are all near 1.0 (R^2>0.995). The correlation coefficient between p-fixed and p-coupled sediment ^{231}Pa/^{230}Th activity ratios in CTRL is 0.99 and the regression coefficient is 0.9 (R^2=0.98) (Fig. 4a). This is expected because the particle fields used in p-fixed version are the climatology of the particle fields used in the p-coupled version. Therefore, under the same climate forcing, p-fixed and p-coupled version of ^{231}Pa and ^{230}Th should be very similar. For the discussion of results in CTRL below, we only discuss the p-fixed ^{231}Pa and ^{230}Th.

The residence time of both ^{231}Pa and ^{230}Th in CTRL are comparable with observations. The residence time is calculated as the ratio of global average total isotope activity and the radioactive ingrowth of the isotope. Residence time in CTRL is 118 yr for ^{231}Pa and 33 yr for ^{230}Th (Table 2), which are of the same magnitude as 111 yr for ^{231}Pa and 26 yr for ^{230}Th in observation (Yu et al., 1996).

CTRL can simulate the general features of dissolved water column ^{231}Pa and ^{230}Th activities. Dissolved ^{231}Pa and ^{230}Th activities increase with depth in CTRL, as shown in two GEOTRACES transects (Deng et al., 2014; Hayes et al., 2015) in the Atlantic (Fig. 2 and 3). The dissolved ^{231}Pa and ^{230}Th activities in CTRL are also at the same order of magnitude as in observations in the most of the ocean, except that simulated values are larger than observations in abyssal, which is also the case in Siddall et al., (2005) and Rempfer et al., (2017) (their Fig. 2 and 3, experiment Re3d). Our model is unable to simulate the realistic dissolved ^{231}Pa and ^{230}Th activities in abyssal because boundary scavenging and sediment resuspensions are not included in our model. With boundary scavenging and sediment resuspensions added, dissolved ^{231}Pa and ^{230}Th activities in the abyssal should be reduced (Rempfer et al., 2017).

A more quantitative model-data comparison is shown in Fig. 5. The linear regression coefficient, an indication of model ability to simulate ^{231}Pa and ^{230}Th activity (Dutay et al., 2009), is near 1.0 for dissolved ^{231}Pa and ^{230}Th (1.02 for $[^{231}Pa]_d$ and 1.14 for $[^{230}Th]_d$), suggesting that CTRL can simulate the dissolved ^{231}Pa and ^{230}Th in good agreement with observations. However, the simulation of the particulate activity is not as good as the dissolved activity. Particulate activity is overall larger than observations in the surface ocean and smaller than observation

Deleted: (Fig. 2e-h)
Deleted: abiotic
Deleted: biotic
Deleted: (N=7879 points)
Deleted: between them
Deleted: abiotic
Deleted: biotic
Deleted: for the present day.
Deleted: abiotic
Deleted: biotic
Deleted: abiotic
Deleted: 1
Deleted: the
Deleted: Both d
Deleted: and particulate activities for
Deleted: except in the regions of deep water formation
Deleted: the zonal mean Atlantic dissolved and particulate ^{231}Pa and ^{230}Th activities (Fig. 2a-d).
Deleted: and particulate
Deleted:
Deleted: (Colley et al., 1995; Luo et al., 2010; Mangini and Key, 1983; Moran et al., 1997, 2002; Rutgers van der Loeff and Berger, 1993; Vogler et al., 1998; Walter et al., 1997)
Deleted: . Our CTRL shows similar results as in
Deleted: (their Fig. 2). The patterns of dissolved ^{231}Pa and ^{230}Th activities are similar except in the Southern Ocean, where high opal flux effectively removes ^{231}Pa to sediment.
Deleted: 3
Deleted: The correlation between model and observations are significant at 0.01 confidence level for all dissolved and particulate ^{231}Pa and ^{230}Th: $[^{231}Pa]_d$ correlation is 0.65, $[^{230}Th]_d$ correlation is 0.73, $[^{231}Pa]_p$ correlation is 0.33 and $[^{230}Th]_p$ correlation is 0.62.
Deleted: 14
Deleted: 0
Deleted:
Deleted: somewhat
Deleted: smaller
Deleted: larger

in the deep ocean for both particulate ^{231}Pa and ^{230}Th. The regression coefficient for particulate ^{231}Pa and ^{230}Th is 0.02 for $[^{231}Pa]_p$ and 0.05 for $[^{230}Th]_p$. The poor performance in simulating water column particulate ^{231}Pa and ^{230}Th activities is also in previous modeling studies (Dutay et al., 2009; Siddall et al., 2005), because of similar modelling scheme are applied. However, the simulated $^{231}Pa_p/^{230}Th_p$ is reasonable. The $^{231}Pa_p/^{230}Th_p$ along two GEOTRACES tracks (Fig. 2 and 3) show the similar pattern and magnitude as in Rempfer et al., (2017). Decrease of $^{231}Pa_p/^{230}Th_p$ with depth is well simulated, which is suggested to be caused by the lateral transport of ^{231}Pa from North Atlantic to Southern Ocean by AMOC (Gherardi et al., 2009; Lippold et al., 2011, 2012a; Luo et al., 2010; Rempfer et al., 2017).

The sediment $^{231}Pa/^{230}Th$ in CTRL is overall consistent with observations (references of observations are listed in Table 3). The North Atlantic shows low sediment $^{231}Pa/^{230}Th$ activity ratio as in observations because ^{231}Pa is more subject to transport southward to the Southern Ocean by active ocean circulation than ^{230}Th because of longer residence time. The Southern Ocean maximum in the sediment $^{231}Pa/^{230}Th$ activity ratio is also simulated in CTRL. High opal fluxes in the Southern Ocean, which preferentially removes ^{231}Pa into sediment ($K_{opal}^{231Pa} > K_{opal}^{230Th}$) (Chase et al., 2002), leading to increased sediment $^{231}Pa/^{230}Th$ activity ratio. In addition, upwelling in the Southern Ocean brings up deep water enriched with ^{231}Pa, which is transported from the North Atlantic, to shallower depth and further contribute to the scavenging. CTRL can also produce higher sediment $^{231}Pa/^{230}Th$ activity ratio in regions with high particle production (e.g. the Eastern equatorial Pacific, the North Pacific and the Indian Ocean) due to the "particle flux effect". Specifically, in North Atlantic, the distribution of sediment $^{231}Pa/^{230}Th$ matches the distribution of particle, especially opal, production: sediment $^{231}Pa/^{230}Th$ is higher where opal production is high, and vice versa.

4.2 Sensitivity on partition coefficient K

In this section, we show model sensitivity on partition coefficient by increasing and decreasing the partition coefficient, K, by a factor of 5, but keep the

Deleted: dissolved

Deleted: 14

Deleted: 42

Deleted: (Fig. 3)

Deleted: This

Deleted: also similar

Deleted:

Deleted: One may think the performance of simulating $[^{231}Pa]_p$ and $[^{230}Th]_p$ can be improved by tuning model parameter: partition coefficient k. However, under current modeling scheme, changing partition coefficient k will have limited influenced on $[^{231}Pa]_p$ and $[^{230}Th]_p$, which will be discussed in section 4.2.

Deleted: activity ratios

Deleted:

Deleted: (Anderson et al., 1983, 1990, 1994; Bacon and Rosholt, 1982; Francois et al., 1993; Frank, 1996; Frank et al., 1994; Ku et al., 1972; Müller and Mangini, 1980; Schmitz et al., 1986; Scholten et al., 1995; Shimmield et al., 1986; Shimmield and Price, 1988; Walter et al., 1997; Yang et al., 1986; Yong-Liang Yang et al., 1995; Yong Lao et al., 1992; Yu et al., 1996)

Deleted: ,

Deleted: which is caused by

Deleted: h

Deleted: ,

Deleted: as well as

Deleted: However, this particle flux effect is less effective in the North Atlantic than in the North Pacific and the Indian Ocean due to active deep ocean circulation transporting ^{231}Pa southward in the Atlantic (Yu et al., 1996).

relative ratio for different particles the same (Table 2). Our model shows similar model sensitivity as in Siddall et al., (2005) as discussed below.

Increasing K will decrease water column dissolved ^{231}Pa and ^{230}Th activities but won't change particulate ^{231}Pa and ^{230}Th too much (Fig. 6). Larger K will lead to more ^{231}Pa and ^{230}Th attached to particles and further buried into sediment, which increases the sink for the ^{231}Pa and ^{230}Th budget. With the sources for ^{231}Pa and ^{230}Th staying the same, dissolved ^{231}Pa and ^{230}Th will be reduced. Increasing K will also reduce the vertical gradient of dissolved ^{231}Pa and ^{230}Th as reversible scavenging act as the vertical transport and increase this vertical transport can decrease the vertical gradient. However, change in the particulate ^{231}Pa and ^{230}Th is small. As stated in Siddall et al., (2005), if we neglect the transport term and the decay term in Eq. (3) and assume particulate phase activity at the surface as 0, when reach equilibrium, the activity of particulate phase will be as in Eq. (7). The particulate phase activity only depends on the production rate, the particle settling velocity and depth. The particulate phase activity will increase linearly with depth and any departure from this linear relationship with depth is due to ocean transport, which is suggested by observations (Bacon and Anderson, 1982; Roy-Barman et al., 1996). Therefore, changing K will have limited influence on particulate phase activity.

$$A_p^i(z) = \frac{\beta^i}{w_s} \cdot z \qquad (7)$$

Increasing K will also reduce the spatial gradient in sediment ^{231}Pa/^{230}Th activity ratio and vice versa (Fig. 7). Larger K will decrease the ^{231}Pa and ^{230}Th residence time and most isotopes produced in the water column are removed into sediment locally (Table 2). Therefore, sediment ^{231}Pa/^{230}Th ratio becomes more homogeneous and approaching the production ration of 0.093 (Fig. 7b). The sediment ^{231}Pa/^{230}Th activity ratio in EXP_1 and EXP_2 departures from observations significantly, suggesting the partition coefficient in CTRL is of the right magnitude.

Deleted: 1

Deleted: to that

Deleted: 5

Deleted: 5

Deleted: 5

Deleted: 6

Deleted: 1

Deleted: 6

4.3. Sediment $^{231}Pa/^{230}Th$ ratio in HOSING

Potential changes in the export of biogenic particles makes using $^{231}Pa/^{230}Th$ ratio to reconstructing AMOC strength under debate. In response to freshwater perturbation in the North Atlantic, both biological productivity and AMOC strength will change and will influence sediment $^{231}Pa/^{230}Th$. Our model with p-fixed and p-coupled ^{231}Pa and ^{230}Th can help detangle these two effects. In this section, we examine the sediment $^{231}Pa/^{230}Th$ (p-fixed and p-coupled) response in the North Atlantic to fresh water perturbation.

In HOSING, after applying freshwater forcing to the North Atlantic, AMOC strength quickly decreases to a minimum of 2 Sv (AMOC_off) (Fig. 9a). During the AMOC_off state, compared with CTRL with active AMOC (AMOC_on), p-fixed sediment $^{231}Pa/^{230}Th$ shows an overall increase in the North Atlantic and a decrease in the South Atlantic (Fig. 10b) because of the reduced southward transport of ^{231}Pa from the North Atlantic by AMOC, consistent with paleo proxy evidence there (e.g. Gherardi et al., 2005, 2009; McManus et al., 2004). The overall increase of sediment $^{231}Pa/^{230}Th$ ratio in the North Atlantic in response to AMOC collapse can be seen more clearly in the time evolution of the sediment $^{231}Pa/^{230}Th$ ratio averaged from 20°N to 60°N in the North Atlantic (Fig.9b, green). Quantitatively, the $^{231}Pa/^{230}Th$ increases from 0.074 in AMOC_on to 0.098 in AMOC_off in the p-fixed version, approaching the production ration of 0.093. This increase of $^{231}Pa/^{230}Th$ is also in the subtropical North Atlantic from the two sites near Bermuda Rise (Fig. 9e and f), which is of comparable magnitude with the change from LGM to HS1 in reconstructions there (McManus et al., 2004). In addition, the pattern of p-fixed (Fig.10a) sediment $^{231}Pa/^{230}Th$ ratio during the Atlantic in AMOC_off state is similar to the opal distribution (Fig.1b) because, without active circulation, sediment $^{231}Pa/^{230}Th$ ratio is more controlled by particle flux effect, which is similar to Pacific in CTRL. It is further noted that our p-fixed sediment $^{231}Pa/^{230}Th$ ratio in HOSING behaves similarly to that in Siddall et al., (2007).

The overall increase in p-fixed sediment $^{231}Pa/^{230}Th$ ratio in the North Atlantic is not homogenous and the magnitude of the change between AMOC_on and

AMOC_off varies with location because of the distribution of particle flux, especially opal flux (Fig.9 and 10). The maximum increase in p-fixed sediment $^{231}Pa/^{230}Th$ ratio occurs near 40°N western Atlantic, where the opal production in our model is maximum in North Atlantic (Fig. 1b). The sediment $^{231}Pa/^{230}Th$ ratio in this region during AMOC_on is larger than production ratio of 0.093 because opal maximum provides extra ^{231}Pa to this region ("particle flux effect"), which overwhelms the active ocean circulation transporting ^{231}Pa southward outside this region (Fig. 9d, green). During AMOC off, without active ocean circulation, the particle flux effect becomes even stronger because less ^{231}Pa is transported out of the North Atlantic and p-fixed sediment $^{231}Pa/^{230}Th$ ratio gets even larger.

Most regions in the Atlantic, p-coupled sediment $^{231}Pa/^{230}Th$ show similar response to p-fixed $^{231}Pa/^{230}Th$ in HOSING. The evolution of p-fixed and p-coupled sediment $^{231}Pa/^{230}Th$ activity ratio in HOSING are highly correlated (Fig. 11a). The change of sediment $^{231}Pa/^{230}Th$ ratio from AMOC_on to AMOC_off are similar in both p-fixed and p-coupled version (Fig.11b). The correlation between p-fixed and p-coupled sediment $^{231}Pa/^{230}Th$ ratio change is 0.72 (1455points) and the linear regression coefficient is 0.71 (R^2 = 0.52). High correlation between p-fixed and p-coupled response mainly happens over low productivity region (Fig.1, 10, and 11), where circulation effect on sediment $^{231}Pa/^{230}Th$ is more important than the particle change in HOSING.

However, the responses of p-fixed and p-coupled sediment $^{231}Pa/^{230}Th$ to the fresh water forcing can differ significantly in high productivity regions because of the change of productivity. With persistent freshwater forcing in the North Atlantic, most regions in the North Atlantic show reduced production of $CaCO_3$, opal and POC (Fig. 8). Productivity in North Atlantic is suggested to be halved during AMOC collapse because of increased stratification, which reduces nutrient supply from deep ocean (Schmittner, 2005). In our model, the productivity in mid-latitude North Atlantic is indeed greatly reduced after the freshwater forcing. For example, opal production from 30°N-50°N in the Atlantic at the end of HOSING is reduced by 50%~90% of its original value in CTRL. However, opal production increases in high latitude North Atlantic at north of 50°N. The pattern of opal production changes

Deleted: With the AMOC collapsing, the $^{231}Pa/^{230}Th$ ratio tends to increase over most of the North Atlantic, consistent with paleo proxy evidence there. In HOSING, after applying extra freshwater to the North Atlantic, AMOC strength quickly decreases to a minimum of 2 Sv at around year 300 (AMOC_off)(Fig. 7a). During the AMOC_off state, compared with CTRL of active AMOC (AMOC_on), both abiotic and biotic sediment $^{231}Pa/^{230}Th$ ratio shows an overall increase in the North Atlantic and a decrease in the South Atlantic (Fig. 8b and d) because of the reduced southward transport of ^{231}Pa from the North Atlantic by AMOC. In most area of the Atlantic, the evolution of abiotic and biotic sediment $^{231}Pa/^{230}Th$ activity ratio in HOSING are highly correlated (Fig. 9a). The change of sediment $^{231}Pa/^{230}Th$ ratio from AMOC_on to AMOC_off are similar in abotic and biotic version (Fig.9b). The correlation between abiotic and biotic sediment $^{231}Pa/^{230}Th$ ratio change is 0.72 (1455points) and the linear regression coefficient is 0.71 (R^2 = 0.52). This suggests that abiotic sediment $^{231}Pa/^{230}Th$ activity ratio can capture the major feature of biotic $^{231}Pa/^{230}Th$ activity ratio in our model and also circulation effect on sediment $^{231}Pa/^{230}Th$ activity ratio is more dominant than the biological effect in HOSING. The pattern of abiotic (Fig.8a) sediment $^{231}Pa/^{230}Th$ ratio in the Atlantic in AMOC_off state is similar to the opal distribution (Fig.1b) because, without active circulation, sediment $^{231}Pa/^{230}Th$ ratio is more controlled by particle flux effect, which is similar to the case in the Pacific in CTRL. The overall increase of sediment $^{231}Pa/^{230}Th$ ratio in the North Atlantic in response to AMOC collapse can be seen more clearly in the time evolution of the sediment $^{231}Pa/^{230}Th$ ratio averaged from 20°N to 60°N in the North Atlantic in both the abiotic and biotic $^{231}Pa/^{230}Th$ (Fig.7b). Quantitatively, the $^{231}Pa/^{230}Th$ increases from 0.074 (0.074) in AMOC_on to 0.098 (0.095) in AMOC_off in the abiotic (biotic) version (Fig. 7b). Both abiotic and biotic version show average sediment $^{231}Pa/^{230}Th$ ratio in the North Atlantic near the production ratio of 0.093. This increase of $^{231}Pa/^{230}Th$ in both abiotic and biotic versions is also seen in the subtropical North Atlantic from the two sites near Bermuda Rise (Fig. 7e and f), which is, of comparable magnitude with the change from LGM to HS1 in reconstructions there (McManus et al., 2004). It is further noted that our abiotic sediment $^{231}Pa/^{230}Th$ ratio in HOSING behaves similarly to that in Siddall et al., (2007). ... [5]

Deleted: T

Deleted: abiotic

Deleted: biotic

Deleted: ratio

Deleted: collapse of AMOC

Deleted: show similar behavior over most ocean region of low productivity but with high opal production region shifts northward in HOSING (Fig. 8 d, e and f). The particle flux change will influence sediment ^{231}Pa/^{230}Th as discussed below.

In subpolar region, the opal productivity increases during AMOC_off and will result an increase in sediment ^{231}Pa/^{230}Th, which is enhance the increase of sediment ^{231}Pa/^{230}Th caused by reduced AMOC. Therefore, the increase in p-coupled sediment ^{231}Pa/^{230}Th between AMOC_off and AMOC_on is larger than p-fixed sediment ^{231}Pa/^{230}Th (Fig.9c).

In the mid-latitude North Atlantic, the opal productivity decreases during AMOC_off and will lead to a decrease in sediment ^{231}Pa/^{230}Th, which is opposite to the effect of reduced AMOC. Therefore, p-coupled sediment ^{231}Pa/^{230}Th shows an initial decrease in first 200 years (Fig.9 d, e, and f, red dash) caused by the reduced opal productivity. But this decrease trend is reversed eventually, suggesting the influence of particle flux change is overwhelmed by the effect of reduced AMOC. It the long run, most regions in the subtropical and mid-latitude Atlantic show increased sediment ^{231}Pa/^{230}Th in HOSING, indicating the dominant effect of reduced AMOC. But sediment ^{231}Pa/^{230}Th at 40°N west Atlantic, where opal productivity is maximum in AMOC_on, show a decrease from AMOC_on to AMOC_off. During AMOC_on, the opal productivity maximum at 40°N west Atlantic lead to regional maximum sediment ^{231}Pa/^{230}Th because of the particle flux effected, which has been explained previously. During AMOC_off, this opal productivity maximum is eliminated and no more extra ^{231}Pa is supplied by surroundings to this region. The decrease in sediment ^{231}Pa/^{230}Th caused by productivity change is larger than the increase caused by the reduced AMOC. Therefore, sediment ^{231}Pa/^{230}Th experienced a decrease from AMOC_on to AMOC_off. Our results suggest that although the circulation effect is more dominant than the particle change in controlling sediment ^{231}Pa/^{230}Th on long time scale in most of North Atlantic, particle flux change can be important on short time scale and in high productivity regions. Therefore, we should be cautious when using sediment ^{231}Pa/^{230}Th to reconstruct AMOC variations in the past.

Formatted: Superscript

Formatted: Not Superscript/ Subscript

It is suggested that the particulate $^{231}Pa/^{230}Th$ response to the change of AMOC depends on the location and depth. Above 2km and high latitude North Atlantic, particulate $^{231}Pa/^{230}Th$ decreases with the increased AMOC (Rempfer et al., 2017). Our results are consistent with this finding (Fig. 12 a and b). Both p-fixed and p-coupled particulate $^{231}Pa/^{230}Th$ show similar patterns of change between AMOC_on and AMOC_off: decrease in particulate $^{231}Pa/^{230}Th$ at shallow depth and north of 60°N and increase in particulate $^{231}Pa/^{230}Th$ below 2km and south of 60°N during AMOC_off. Therefore, sediment depth should be taken into consideration when interpreting sediment $^{231}Pa/^{230}Th$. Since the pattern in p-coupled is similar to the pattern in p-fixed, the opposite particulate $^{231}Pa/^{230}Th$ changes in shallow and deep North Atlantic is associated with AMOC. During AMOC_on, upper limb of AMOC (about upper 1km) transport water northward, which provides extra ^{231}Pa to North Atlantic and particulate $^{231}Pa/^{230}Th$ is larger than the production ratio of 0.093. In contrast, the lower limb of AMOC (2km-3km) features southward transport, which transports ^{231}Pa to the Southern Ocean and particulate $^{231}Pa/^{230}Th$ is smaller than the production ratio of 0.093 (Fig. 12 solid). During AMOC_off, ocean transport of 231Pa is greatly reduced. Therefore, shallow (deep) depth experiences a decrease (increase) in particulate $^{231}Pa/^{230}Th$ and the vertical gradient in the particulate $^{231}Pa/^{230}Th$ is also greatly reduced (Fig. 12 c). Our results support that the depth dependence of particulate $^{231}Pa/^{230}Th$ is mainly caused by lateral transport of ^{231}Pa by circulation (Gherardi et al., 2009; Lippold et al., 2011, 2012a; Luo et al., 2010; Rempfer et al., 2017).

Overall, our model is able to simulate the correct magnitude of the sediment $^{231}Pa/^{230}Th$ ratio response to the freshwater forcing. Change of circulation has the dominant influence on sediment $^{231}Pa/^{230}Th$ on long time scale over most of regions in the hosing experiment, although the detailed difference between p-fixed and p-coupled sediment $^{231}Pa/^{230}Th$ ratio response to freshwater forcing in different locations can be complicated.

5. Summary

Formatted: Superscript

Formatted: Superscript

Formatted: Superscript

Deleted: Productivity in North Atlantic is suggested to be halved during AMOC collapse because of increased stratification, which reduces nutrient supply from deep ocean (Schmittner, 2005). In the CESM, the productivity in mid-latitude North Atlantic is indeed greatly reduced after the freshwater forcing. For example, at year 100 in HOSING, opal production from 30°N-50°N in the Atlantic is reduced by 50%~90% of its original value in CTRL (not shown). Therefore, in the first 100 years in HOSING, most biotic sediment $^{231}Pa/^{230}Th$ ratio show an initial decrease in the North Atlantic from the subtropics to the mid-latitude (Fig.7 d, e, and f, red dash). In the subpolar region, the productivity is increased in the model, leading to an initial increase of biotic sediment $^{231}Pa/^{230}Th$ ratio (Fig.7c). Furthermore, the detailed pattern of the difference between AMOC_off and AMOC_on in sediment $^{231}Pa/^{230}Th$ ratio is different.

Deleted: For example, the region (near 40°N west Atlantic), which has the maximum increase from AMOC_on to AMOC_off in abiotic sediment $^{231}Pa/^{230}Th$ ratio discussed above, shows a decrease in biotic sediment $^{231}Pa/^{230}Th$ ratio (Fig. 7d and Fig.8d) because there is no more opal maximum in this region in AMOC_off. A detailed discussion of the difference between abiotic and biotic sediment $^{231}Pa/^{230}Th$ ratio in different regions is beyond the scope of this paper.

Deleted: change of AMOC

Deleted: ,

Deleted: abiotic

Deleted: biotic

Deleted:

Formatted: Indent: First line: 0"

Deleted:

^{231}Pa and ^{230}Th have been implemented in the ocean model of the CESM in both the p-coupled and p-fixed forms. Our control experiment under present day climate forcing is able to simulate most ^{231}Pa and ^{230}Th water column activity and sediment ^{231}Pa/^{230}Th activity ratio consistent with observations by using the parameters that are suggested by Chase et al., (2002) and used in Siddall et al. (2005). Our sensitivity experiments with varying parameters suggest that these parameters are of the right magnitude.

Deleted: to
Deleted: biotic
Deleted: abiotic
Deleted: both

Furthermore, our model is able to simulate the overall sediment ^{231}Pa/^{230}Th ratio change in the North Atlantic with a magnitude comparable to the reconstruction in response to the collapse of AMOC, although the detailed response can be complicated in different regions. Finally, the p-fixed form is able to capture many major features of that of the p-coupled form over large ocean areas on long time scale, although the two forms can also differ significantly in some regions, especially the region with high opal productivity. Therefore, with both p-fixed and p-coupled ^{231}Pa and ^{230}Th, our model can serve as a useful tool to improve our understanding of the processes of ^{231}Pa and ^{230}Th and also interpretations of sediment ^{231}Pa/^{230}Th reconstructions for past ocean circulation and climate changes.

Formatted: Indent: First line: 0.5"
Deleted: regional
Deleted: abiotic
Deleted: biotic
Deleted: large
Deleted: abiotic
Deleted: biotic

Code availability:

The ^{231}Pa and ^{230}Th isotope source code of both p-fixed and p-coupled versions for CESM1.3 is included as supplementary material here.

Deleted: abiotic
Deleted: biotic

Acknowledgement:

This work is supported by US NSF P2C2 program and the National Science Foundation of China No. 41630527. Computing resources (ark:/85065/d7wd3xhc) were provided by the Climate Simulation Laboratory at NCAR's Computational and Information Systems Laboratory, sponsored by the National Science Foundation and other agencies.

Deleted: projects NSF1401778
Deleted: and NSF1401802, DOE DE-SC0006744
Deleted: 41130105

References:

Anderson, R. F., Bacon, M. P. and Brewer, P. G.: Removal of230Th and231Pa from the open ocean, Earth Planet. Sci. Lett., 62(1), 7–23, doi:10.1016/0012-821X(83)90067-5, 1983.

Anderson, R. F., Lao, Y., Broecker, W. S., Trumbore, S. E., Hofmann, H. J. and Wolfli, W.: Boundary scavenging in the Pacific Ocean: A comparison of 10Be and 231Pa, Earth Planet. Sci. Lett., 96(3–4), 287–304, doi:10.1016/j.cognition.2008.05.007, 1990.

Anderson, R. F., Fleisher, M. Q., Biscaye, P. E., Kumar, N., Dittrich, B., Kubik, P. and Suter, M.: Anomalous boundary scavenging in the Middle Atlantic Bight: evidence from 230Th, 231Pa, 10Be and 210Pb, Deep. Res. Part II, 41(2–3), 537–561, doi:10.1016/0967-0645(94)90034-5, 1994.

Armstrong, R. A., Lee, C., Hedges, J. I., Honjo, S. and Wakeham, S. G.: A new, mechanistic model for organic carbon fluxes in the ocean based on the quantitative association of POC with ballast minerals, Deep. Res. Part II Top. Stud. Oceanogr., 49(1–3), 219–236, doi:10.1016/S0967-0645(01)00101-1, 2002.

Arsouze, T., Dutay, J.-C., Lacan, F. and Jeandel, C.: Reconstructing the Nd oceanic cycle using a coupled dynamical – biogeochemical model, Biogeosciences, 6(12), 2829–2846, doi:10.5194/bg-6-2829-2009, 2009.

Bacon, M. and Anderson, R.: Distribution of Thorium Isotopes between dissolved and particulate forms in the deep sea, J. Geophys. Res. …, 87(1), 2045–2056, 1982.

Bacon, M. P. and Rosholt, J. N.: Accumulation rates of 230Th, 231Pa, and some transition metals on the Bermuda Rise, Geochim. Cosmochim. Acta, 46, 651–666, 1982.

Bacon, M. P., Huh, C. A. and Moore, R. M.: Vertical profiles of some natural radionuclides over the Alpha Ridge, Arctic Ocean, Earth Planet. Sci. Lett., 95(1–2), 15–22, doi:10.1016/0012-821X(89)90164-7, 1989.

Bradtmiller, L. I., Anderson, R. F., Fleisher, M. Q. and Burckle, L. H.: Opal burial in the equatorial Atlantic Ocean over the last 30 ka: Implications for glacial-interglacial changes in the ocean silicon cycle, Paleoceanography, 22(4), 1–15, doi:10.1029/2007PA001443, 2007.

Bradtmiller, L. I., McManus, J. F. and Robinson, L. F.: 231Pa/230Th evidence for a weakened but persistent Atlantic meridional overturning circulation during Heinrich Stadial 1, Nat. Commun., 5, 5817, doi:10.1038/ncomms6817, 2014.

Burckel, P., Waelbroeck, C., Luo, Y., Roche, D. M., Pichat, S., Jaccard, S. L., Gherardi, J., Govin, A., Lippold, J. and Thil, F.: Changes in the geometry and strength of the Atlantic meridional overturning circulation during the last glacial (20-50 ka), Clim. Past, 12(11), 2061–2075, doi:10.5194/cp-12-2061-2016, 2016.

Chase, Z. and Robert F, A.: Comment on “On the importance of opal, carbonate, and lithogenic clays in scavenging and fractionating 230Th, 231Pa and 10Be in the ocean” by S. Luo and T.-L. Ku, Earth Planet. Sci. Lett., 220(1–2), 201–211, doi:10.1016/S0012-821X(04)00027-5, 2004.

Chase, Z., Anderson, R. F., Fleisher, M. Q. and Kubik, P. W.: The influence of particle composition and particle flux on scavenging of Th , Pa and Be in the ocean, Earth Planet. Sci. Lett., 204(1–2), 215–229, doi:10.1016/S0012-821X(02)00984-6, 2002.

Cochran, J. K., Livingston, H. D., Hirschberg, D. J. and Surprenant, L. D.: Natural and anthropogenic radionuclide distributions in the northwest Atlantic Ocean, Earth Planet. Sci. Lett., 84(2–3), 135–152, doi:10.1016/0012-821X(87)90081-1, 1987.

Cochran, J. K., Hirschberg, D. J., Livingston, H. D., Buesseler, K. O. and Key, R. M.: Natural and anthropogenic radionuclide distributions in the Nansen Basin, Artic Ocean: Scavenging rates and circulation timescales, Deep. Res. Part II, 42(6), 1495–1517, doi:10.1016/0967-0645(95)00051-8, 1995.

Colley, S., Thomson, J. and Newton, P. P.: Detailed Th-230, Th-232 and Pb-210 fluxes recorded by the 1989/90 BOFS sediment trap time-series at 48N, 20W, Deep - Sea Res. Part I - Oceanogr. Res. Pap., 42(6), 833–848, 1995.

Coppola, L., Roy-Barman, M., Mulsow, S., Povinec, P. and Jeandel, C.: Thorium isotopes as tracers of particles dynamics and deep water circulation in the Indian sector of the Southern Ocean (ANTARES IV), Mar. Chem., 100(3–4 SPEC. ISS.), 299–313, doi:10.1016/j.marchem.2005.10.019, 2006.

Danabasoglu, G., Bates, S. C., Briegleb, B. P., Jayne, S. R., Jochum, M., Large, W. G., Peacock, S. and Yeager, S. G.: The CCSM4 ocean component, J. Clim., 25(5), 1361–1389, doi:10.1175/JCLI-D-11-00091.1, 2012.

DeMaster, D. J.: The marine budgets of silica and 32Si, Yale., 1979.

Deng, F., Thomas, A. L., Rijkenberg, M. J. A. and Henderson, G. M.: Controls on seawater 231Pa, 230Th and 232Th concentrations along the flow paths of deep waters in the Southwest Atlantic, Earth Planet. Sci. Lett., 390, 93–102, doi:10.1016/j.epsl.2013.12.038, 2014.

Doney, S. C., Lima, I., Feely, R. A., Glover, D. M., Lindsay, K., Mahowald, N., Moore, J. K. and Wanninkhof, R.: Mechanisms governing interannual variability in upper-ocean inorganic carbon system and air-sea CO2 fluxes: Physical climate and atmospheric dust, Deep. Res. Part II Top. Stud. Oceanogr., 56(8–10), 640–655, doi:10.1016/j.dsr2.2008.12.006, 2009.

Dutay, J.-C., Lacan, F., Roy-Barman, M. and Bopp, L.: Influence of particle size and type on 231 Pa and 230 Th simulation with a global coupled biogeochemical-ocean general circulation model: A first approach, Geochemistry, Geophys. Geosystems, 10(1), doi:10.1029/2008GC002291, 2009.

Edmonds, H. N., Moran, S. B., Hoff, J. A., Smith, J. N. and Edwards, R. L.: Protactinium-231 and Thorium-230 Abundances and High Scavenging Rates in the Western Arctic Ocean, Science (80-.)., 280(5362), 405–407, doi:10.1126/science.280.5362.405, 1998.

Edmonds, H. N., Moran, S. B., Cheng, H. and Edwards, R. L.: 230Th and 231Pa in the Arctic Ocean: Implications for particle fluxes and basin-scale Th/Pa fractionation, Earth Planet. Sci. Lett., 227(1–2), 155–167, doi:10.1016/j.epsl.2004.08.008, 2004.

Francois, R., Bacon, M. P., Altabet, M. A. and Labeyrie, L. D.: Glacial/interglacial changes in sediment rain rate in the SW Indian Sector of subantarctic Waters as recorded by 230Th, 231Pa, U, and d15N, Paleoceanography, 8(5), 611–629, doi:10.1029/93PA00784, 1993.

Frank, M.: Reconstruction of Late Quaternary environmental conditions applying the natural radionuclides 230Th, 10Be, 231Pa and 238U: A study of deep-sea sediments from the eastern sector of the Antarctic Circumpolar Current System, Alfred Wegener Institute for Polar and Marine Research., 1996.

Frank, M., Eisenhauer, A., Kubik, P. W., Dittrich-hannen, B. and Segl, M.: Beryllium 10, thorium 230, and protactinium 231 in Galapagos microplate sediments: Implications of hydrothermal activity and paleoproductivity changes during the last 100,000 years, Palaeogeography, 9(4), 559–578, 1994.

Geibert, W. and Usbeck, R.: Adsorption of thorium and protactinium onto different particle types: Experimental findings, Geochim. Cosmochim. Acta, 68(7), 1489–1501, doi:10.1016/j.gca.2003.10.011, 2004.

Gherardi, J., Labeyrie, L., Mcmanus, J., Francois, R., Skinner, L. and Cortijo, E.: Evidence from the Northeastern Atlantic basin for variability in the rate of the meridional overturning circulation through the last deglaciation, Earth Planet. Sci. Lett., 240(3–4), 710–723, doi:10.1016/j.epsl.2005.09.061, 2005.

Gherardi, J.-M., Labeyrie, L., Nave, S., Francois, R., McManus, J. F. and Cortijo, E.: Glacial-interglacial circulation changes inferred from 231 Pa/ 230 Th sedimentary record in the North Atlantic region, Paleoceanography, 24(2), doi:10.1029/2008PA001696, 2009.

Guo, L., Santschi, P. H., Baskaran, M. and Zindler, A.: Distribution of dissolved and particulate 230Th and 232Th in seawater from the Gulf of Mexico and off Cape Hatteras as measured by SIMS, Earth Planet. Sci. Lett., 133(1), 117–128, 1995.

Gutjahr, M., Frank, M., Stirling, C. H., Keigwin, L. D. and Halliday, a. N.: Tracing the Nd isotope evolution of North Atlantic Deep and Intermediate Waters in the western North Atlantic since the Last Glacial Maximum from Blake Ridge sediments, Earth Planet. Sci. Lett., 266(1–2), 61–77, doi:10.1016/j.epsl.2007.10.037, 2008.

Hall, I. R., Moran, S. B., Zahn, R., Knutz, P. C., Shen, C.-C. and Edwards, R. L.: Accelerated drawdown of meridional overturning in the late-glacial Atlantic triggered by transient pre-H event freshwater perturbation, Geophys. Res. Lett., 33(16), L16616, doi:10.1029/2006GL026239, 2006.

Hayes, C. T., Anderson, R. F., Fleisher, M. Q., Serno, S., Winckler, G. and Gersonde, R.: Quantifying lithogenic inputs to the North Pacific Ocean using the long-lived thorium isotopes, Earth Planet. Sci. Lett., 383, 16–25, doi:10.1016/j.epsl.2013.09.025, 2013.

Hayes, C. T., Anderson, R. F., Fleisher, M. Q., Huang, K. F., Robinson, L. F., Lu, Y., Cheng, H., Edwards, R. L. and Moran, S. B.: ^{230}Th and ^{231}Pa on GEOTRACES GA03, the U.S. GEOTRACES North Atlantic transect, and implications for modern and paleoceanographic chemical fluxes, Deep. Res. Part II Top. Stud. Oceanogr., 116, 29–41, doi:10.1016/j.dsr2.2014.07.007, 2015.

Henderson, G. M. and Anderson, R. F.: The U-series toolbox for paleoceanography, Rev. Mineral. Geochemistry, 52(1), 493–531, doi:10.2113/0520493, 2003.

Henderson, G. M., Heinze, C., Anderson, R. F. and Winguth, A. M. E.: Global distribution of the 230Th flux to ocean sediments constrained by GCM modelling, Deep. Res. Part I Oceanogr. Res. Pap., 46(11), 1861–1893, doi:10.1016/S0967-0637(99)00030-8, 1999.

Hoffmann, S. S., McManus, J. F., Curry, W. B. and Brown-Leger, L. S.: Persistent export of 231Pa from the deep central Arctic Ocean over the past 35,000 years., Nature, 497(7451), 603–6, doi:10.1038/nature12145, 2013.

Hsieh, Y. Te, Henderson, G. M. and Thomas, A. L.: Combining seawater 232Th and 230Th concentrations to determine dust fluxes to the surface ocean, Earth Planet.

Sci. Lett., 312(3–4), 280–290, doi:10.1016/j.epsl.2011.10.022, 2011.

Huh, C. A. and Beasley, T. M.: Profiles of dissolved and particulate thorium isotopes in the water column of coastal Southern California, Earth Planet. Sci. Lett., 85(1–3), 1–10, doi:10.1016/0012-821X(87)90016-1, 1987.

Hurrell, J. W., Holland, M. M., Gent, P. R., Ghan, S., Kay, J. E., Kushner, P. J., Lamarque, J. F., Large, W. G., Lawrence, D., Lindsay, K., Lipscomb, W. H., Long, M. C., Mahowald, N., Marsh, D. R., Neale, R. B., Rasch, P., Vavrus, S., Vertenstein, M., Bader, D., Collins, W. D., Hack, J. J., Kiehl, J. and Marshall, S.: The community earth system model: A framework for collaborative research, Bull. Am. Meteorol. Soc., 94(9), 1339–1360, doi:10.1175/BAMS-D-12-00121.1, 2013.

Jahn, A., Lindsay, K., Giraud, X., Gruber, N., Otto-Bliesner, B. L., Liu, Z. and Brady, E. C.: Carbon isotopes in the ocean model of the Community Earth System Model (CESM1), Geosci. Model Dev., 8(8), 2419–2434, doi:10.5194/gmd-8-2419-2015, 2015.

Jonkers, L., Zahn, R., Thomas, A., Henderson, G., Abouchami, W., Fran??ois, R., Masque, P., Hall, I. R. and Bickert, T.: Deep circulation changes in the central South Atlantic during the past 145 kyrs reflected in a combined 231Pa/230Th, Neodymium isotope and benthic dC13 record, Earth Planet. Sci. Lett., 419, 14–21, doi:10.1016/j.epsl.2015.03.004, 2015.

Keigwin, L. D. and Boyle, E. A.: Did North Atlantic overturning halt 17,000 years ago?, Paleoceanography, 23(1), 1–5, doi:10.1029/2007PA001500, 2008.

Kriest, I.: Different parameterizations of marine snow in a 1D-model and their influence on representation of marine snow, nitrogen budget and sedimentation, Deep. Res. Part I Oceanogr. Res. Pap., 49(12), 2133–2162, doi:10.1016/S0967-0637(02)00127-9, 2002.

Ku, T. L.: Uranium series disequilibrium in deep sea sediments, Columbia., 1966.

Ku, T. L., Bischoff, J. L. and Boersma, A.: Age studies of Mid-Atlantic Ridge sediments near 42??N and 20??N, Deep. Res. Oceanogr. Abstr., 19(3), 233–247, doi:10.1016/0011-7471(72)90033-2, 1972.

Kumar, N.: Trace metals and natural radionuclides as tracers of ocean productivity, Columbia., 1994.

Kumar, N., Gwiazda, R., Anderson, R. F. and Froelich, P. N.: 231Pa/230Th ratios in sediments as a proxy for past changes in Southern Ocean productivity, Nature, 362, 45–48, doi:10.1038/362045a0, 1993.

Large, W. G. and Yeager, S. G.: The global climatology of an interannually varying air–sea flux data set, Clim. Dyn., 33(2–3), 341–364, doi:10.1007/s00382-008-0441-3, 2008.

Lippold, J., Grützner, J., Winter, D., Lahaye, Y., Mangini, A. and Christi, M.: Does sedimentary 231Pa/230Th from the Bermuda Rise monitor past Atlantic Meridional Overturning Circulation?, Geophys. Res. Lett., 36(12), 1–6, doi:10.1029/2009GL038068, 2009.

Lippold, J., Gherardi, J. M. and Luo, Y.: Testing the ^{231}Pa/^{230}Th paleocirculation proxy: A data versus 2D model comparison, Geophys. Res. Lett., 38(20), 1–7, doi:10.1029/2011GL049282, 2011.

Lippold, J., Mulitza, S., Mollenhauer, G., Weyer, S., Heslop, D. and Christl, M.: Boundary scavenging at the East Atlantic margin does not negate use of 231Pa/

230Th to trace Atlantic overturning, Earth Planet. Sci. Lett., 333–334, 317–331, doi:10.1016/j.epsl.2012.04.005, 2012a.

Lippold, J., Luo, Y., Francois, R., Allen, S. E., Gherardi, J., Pichat, S., Hickey, B. and Schulz, H.: Strength and geometry of the glacial Atlantic Meridional Overturning Circulation, Nat. Geosci., 5(11), 813–816, doi:10.1038/ngeo1608, 2012b.

Long, M. C., Lindsay, K., Peacock, S., Moore, J. K. and Doney, S. C.: Twentieth-century oceanic carbon uptake and storage in CESM1(BGC), J. Clim., 26(18), 6775–6800, doi:10.1175/JCLI-D-12-00184.s1, 2013.

Luo, S. and Ku, T. L.: Oceanic 231Pa/230Th ratio influenced by particle composition and remineralization, Earth Planet. Sci. Lett., 167(3–4), 183–195, doi:10.1016/S0012-821X(99)00035-7, 1999.

Luo, S. D., Ku, T. L., Kusakabe, M., Bishop, J. K. B. and Yang, Y. L.: Tracing particle cycling in the upper ocean with Th-230 and Th-228: An investigation in the equatorial Pacific along 140 degrees W, Deep - Sea Res. Part II - Top. Stud. Oceanogr., 42(2–3), 805–829, doi:10.1016/0967-0645(95)00019-M, 1995.

Luo, Y., Francois, R. and Allen, S.: Sediment 231Pa/230Th as a recorder of the rate of the Atlantic meridional overturning circulation: insights from a 2-D model, Ocean Sci., 6(3), 381–400, doi:10.5194/os-6-381-2010, 2010.

Mangini, A. and Diester-Hass, L.: Excess Th-230 in sediments off NW Africa traces upwelling during the past 130,000 years, in Coastal upwelling: Its sedimentary records, edited by E. Suess and J. Thiede, pp. 455–470, Plenum., 1983.

Mangini, A. and Key, R. M.: A 230Th profile in the Atlantic Ocean, Earth Planet. Sci. Lett., 62(3), 377–384, doi:10.1016/0012-821X(83)90008-0, 1983.

Mangini, A. and Sonntag, C.: 231Pa dating of deep-sea cores via 227Th counting, Earth Planet. Sci. Lett., 37(2), 251–256, 1977.

Mangini, A. and U., K.: Depositional history in the Clarion-Clipperton zone during the last 250,000 years: 230Th and 231Pa methods, Geol. Jahrb., 87, 105–121, 1987.

Marchal, O., François, R., Stocker, T. F. and Joos, F.: Ocean thermohaline circulation and sedimentary 231Pa/230Th ratio, Paleoceanography, 15(6), 625–641 [online] Available from: http://onlinelibrary.wiley.com/doi/10.1029/2000PA000496/full (Accessed 19 April 2016), 2000.

McManus, J., Francois, R. and Gherardi, J.: Collapse and rapid resumption of Atlantic meridional circulation linked to deglacial climate changes, Nature, 428(6985), 834–837, 2004.

Moore, J. K. and Braucher, O.: Sedimentary and mineral dust sources of dissolved iron to the World Ocean, Biogeosciences, 5(1994), 631–656, doi:10.5194/bgd-4-1279-2007, 2008.

Moore, J. K., Doney, S. C., Glover, D. M. and Fung, I. Y.: Iron cycling and nutrient-limitation patterns in surface waters of the World Ocean, , 49, 463–507, 2002.

Moore, J. K., Doney, S. C. and Lindsay, K.: Upper ocean ecosystem dynamics and iron cycling in a global three-dimensional model, Global Biogeochem. Cycles, 18(4), doi:10.1029/2004GB002220, 2004.

Moore, J. K., Lindsay, K., Doney, S. C., Long, M. C. and Misumi, K.: Marine Ecosystem Dynamics and Biogeochemical Cycling in the Community Earth System Model [CESM1(BGC)]: Comparison of the 1990s with the 2090s under the RCP4.5 and RCP8.5 Scenarios, J. Clim., 26(23), 9291–9312, doi:10.1175/JCLI-D-12-00566.1, 2013.

Moore, R. M. and Hunter, K. A.: Thorium adsorption in the ocean: reversibility and distribution amongst particle sizes, Geochim. Cosmochim. Acta, 49(11), 2253–2257, doi:10.1016/0016-7037(85)90225-X, 1985.

Moore, W. S.: The thorium isotope content of ocean water, Earth Planet. Sci. Lett., 53(3), 419–426, doi:10.1016/0012-821X(81)90046-7, 1981.

Moran, S. B., Hoff, J. A., Buesseler, K. O. and Edwards, R. L.: High precision 230Th and 232Th in the Norwegian Sea and Denmark by thermal ionization mass spectrometry, , 22(19), 2589–2592, 1995.

Moran, S. B., Charette, M. a., Hoff, J. a., Edwards, R. L. and Landing, W. M.: Distribution of 230Th in the Labrador Sea and its relation to ventilation, Earth Planet. Sci. Lett., 150, 151–160, doi:10.1016/S0012-821X(97)00081-2, 1997.

Moran, S. B., Shen, C.-C., Weinstein, S. E., Hettinger, L. H., Hoff, J. H., E dmonds, H. N. and Edwards, R. L.: Constraints on deep water age and particle flux in the Equatorial and South Atlantic Ocean based on seawater 231Pa and 230Th data, Geophys. Res. Lett., 28(18), 3437–3440 [online] Available from: papers2://publication/uuid/2A811583-B32B-4BD8-B582-EC8B0D96A949, 2001.

Moran, S. B., Shen, C. C., Edmonds, H. N., Weinstein, S. E., Smith, J. N. and Edwards, R. L.: Dissolved and particulate 231Pa and 230Th in the Atlantic Ocean: Constraints on intermediate/deep water age, boundary scavenging, and 231Pa/230Th fractionation, Earth Planet. Sci. Lett., 203(3–4), 999–1014, doi:10.1016/S0012-821X(02)00928-7, 2002.

Müller, P. J. and Mangini, A.: Organic carbon decomposition rates in sediments of the pacific manganese nodule belt dated by 230Th and 231Pa, Earth Planet. Sci. Lett., 51(1), 94–114, doi:10.1016/0012-821X(80)90259-9, 1980.

Negre, C., Zahn, R., Thomas, A. L., Masqué, P., Henderson, G. M., Martínez-Méndez, G., Hall, I. R. and Mas, J. L.: Reversed flow of Atlantic deep water during the Last Glacial Maximum., Nature, 468(7320), 84–88, doi:10.1038/nature09508, 2010.

Nozaki, Y. and Horibe, Y.: Alpha-emitting thorium isotopes in northwest Pacific deep waters, Earth Planet. Sci. Lett., 65(1), 39–50, doi:10.1016/0012-821X(83)90188-7, 1983.

Nozaki, Y. and Nakanishi, T.: 231Pa and 230Th profiles in the open ocean water column, Deep Sea Res. Part A, Oceanogr. Res. Pap., 32(10), 1209–1220, doi:10.1016/0198-0149(85)90004-4, 1985.

Nozaki, Y. and Yamada, M.: Thorium and protactinium isotope distributions in waters of the Japan Sea, Deep Sea Res. Part A, Oceanogr. Res. Pap., 34(8), 1417–1430, 1987.

Nozaki, Y. and Yang, H. S.: Th and Pa isotopes in the waters of the western margin of the pacific near Japan: Evidence for release of228Ra and227Ac from slope sediments, J. Oceanogr. Soc. Japan, 43(4), 217–227, doi:10.1007/BF02109817, 1987.

Nozaki, Y., Horibe, Y. and Tsubota, H.: The water column distribution of thorium isotopes in the western North Pacific, Earth Planet. Sci. Lett., 54(54), 203–216, 1981.

Nozaki, Y., Yang, H.-S. and Yamada, M.: Scavenging of thorium in the ocean, J. Geophys. Res., 92(C1), 772, doi:10.1029/JC092iC01p00772, 1987.

Okubo, A., Obata, H., Nozaki, Y., Yamamoto, Y. and Minami, H.: 230Th in the Andaman Sea: Rapid deep-sea renewal, Geophys. Res. Lett., 31(22), 1–5, doi:10.1029/2004GL020226, 2004.

Okubo, A., Obata, H., Luo, S., Gamo, T., Yamamoto, Y., Minami, H. and Yamada, M.: Particle flux in the twilight zone of the eastern Indian Ocean: A constraint from 234U-230Th and 228Ra-228Th disequilibria, Deep. Res. Part I Oceanogr. Res. Pap., 54(10), 1758–1772, doi:10.1016/j.dsr.2007.06.009, 2007a.

Okubo, A., Obata, H., Gamo, T., Minami, H. and Yamada, M.: Scavenging of 230Th in the Sulu Sea, Deep. Res. Part II Top. Stud. Oceanogr., 54(1–2), 50–59, doi:10.1016/j.dsr2.2006.02.016, 2007b.

Okubo, A., Obata, H., Gamo, T. and Yamada, M.: 230Th and 232Th distributions in mid-latitudes of the North Pacific Ocean: Effect of bottom scavenging, Earth Planet. Sci. Lett., 339–340, 139–150, doi:10.1016/j.epsl.2012.05.012, 2012.

Rempfer, J., Stocker, T. F., Joos, F., Dutay, J.-C. and Siddall, M.: Modelling Nd-isotopes with a coarse resolution ocean circulation model: Sensitivities to model parameters and source/sink distributions, Geochim. Cosmochim. Acta, 75(20), 5927–5950, doi:10.1016/j.gca.2011.07.044, 2011.

Rempfer, J., Stocker, T. F., Joos, F., Lippold, J. and Jaccard, S. L.: New insights into cycling of 231 Pa and 230 Th in the Atlantic Ocean, Earth Planet. Sci. Lett., 468, 27–37, doi:10.1016/j.epsl.2017.03.027, 2017.

Roberts, N. L., McManus, J. F., Piotrowski, A. M. and McCave, I. N.: Advection and scavenging controls of Pa/Th in the northern NE Atlantic, Paleoceanography, 29(6), 668–679, doi:10.1002/2014PA002633, 2014.

Robinson, L. F., Belshaw, N. S. and Henderson, G. M.: U and Th concentrations and isotope ratios in modern carbonates and waters from the Bahamas, Geochim. Cosmochim. Acta, 68(8), 1777–1789, doi:10.1016/j.gca.2003.10.005, 2004.

Roy-Barman, M., Chen, J. H. and Wasserburg, G. J.: 230Th-232Th systematics in the central Pacific Ocean: The sources and the fates of thorium, Earth Planet. Sci. Lett., 139(3–4), 351–363, doi:10.1016/0012-821X(96)00017-9, 1996.

Rutgers van der Loeff, M. M. and Berger, G. W.: Scavenging of 230Th and 231Pa near the antarctic polar front in the South Atlantic, Deep. Res. Part I, 40(2), 339–357, doi:10.1016/0967-0637(93)90007-P, 1993.

Schmittner, A.: Decline of the marine ecosystem caused by a reduction in the Atlantic overturning circulation., Nature, 434(7033), 628–633, doi:10.1038/nature03476, 2005.

Schmitz, W., Mangini, A., Stoffers, P., Glasby, G. P. and Pluger, W. L.: Sediment accumulation rates in the southwestern Pacific Basin and Aitutaki Passage, Mar. Geol., 73(1), 181–190, 1986.

Scholten, J. C., Rutgers van der Loeff, M. M. and Michel, A.: Distribution of 230Th and 231Pa in the water column in relation to the ventilation of the deep Arctic basins, Deep. Res. Part II, 42(6), 1519–1531, doi:10.1016/0967-0645(95)00052-6, 1995.

Scholten, J. C., Fietzke, J., Mangini, A., Garbe-Schönberg, C. D., Eisenhauer, A., Schneider, R. and Stoffers, P.: Advection and scavenging: Effects on 230Th and 231Pa distribution off Southwest Africa, Earth Planet. Sci. Lett., 271(1–4), 159–169, doi:10.1016/j.epsl.2008.03.060, 2008.

Shimmield, G. B. and Price, N. B.: The scavenging of U,230Th and 231Pa during pulsed hydrothermal activity at 20??S, East Pacific Rise, Geochim. Cosmochim. Acta, 52(3), 669–677, doi:10.1016/0016-7037(88)90329-8, 1988.

Shimmield, G. B., Murray, J. W., Thomson, J., Bacon, M. P., Anderson, R. F. and Price, N. B.: The distribution and behaviour of 230Th and 231Pa at an ocean margin, Baja California, Mexico, Geochim. Cosmochim. Acta, 50(11), 2499–2507, doi:10.1016/0016-7037(86)90032-3, 1986.

Siddall, M., Henderson, G. M., Edwards, N. R., Frank, M., Müller, S. a., Stocker, T. F. and Joos, F.: 231Pa/230Th fractionation by ocean transport, biogenic particle flux and particle type, Earth Planet. Sci. Lett., 237(1–2), 135–155, doi:10.1016/j.epsl.2005.05.031, 2005.

Siddall, M., Stocker, T. F., Henderson, G. M., Joos, F., Frank, M., Edwards, N. R., Ritz, S. P. and Müller, S. a.: Modeling the relationship between 231 Pa/ 230 Th distribution in North Atlantic sediment and Atlantic meridional overturning circulation, Paleoceanography, 22(2), n/a-n/a, doi:10.1029/2006PA001358, 2007.

Thomas, A. L., Henderson, G. M. and Robinson, L. F.: Interpretation of the 231Pa/230Th paleocirculation proxy: New water-column measurements from the southwest Indian Ocean, Earth Planet. Sci. Lett., 241(3–4), 493–504, doi:10.1016/j.epsl.2005.11.031, 2006.

Trimble, S. M., Baskaran, M. and Porcelli, D.: Scavenging of thorium isotopes in the Canada Basin of the Arctic Ocean, Earth Planet. Sci. Lett., 222(3–4), 915–932, doi:10.1016/j.epsl.2004.03.027, 2004.

Venchiarutti, C., van der Loeff, M. R. and Stimac, I.: Scavenging of 231Pa and thorium isotopes based on dissolved and size-fractionated particulate distributions at Drake Passage (ANTXXIV-3), Deep. Res. Part II Top. Stud. Oceanogr., 58(25–26), 2767–2784, doi:10.1016/j.dsr2.2010.10.040, 2011.

Vogler, S., Scholten, J., Rutgers van der Loeff, M. M. and Mangini, A.: 230Th in the eastern North Atlantic: the importance of water mass ventilation in the balance of 230Th, Earth Planet. Sci. Lett., 156(1–2), 61–74, doi:10.1016/S0012-821X(98)00011-9, 1998.

Walter, H. J., Rutgers van der Loeff, M. M. and Hoeltzen, H.: Enhanced scavenging of 231Pa relative to 230Th in the South Atlantic south of the Polar Front: Implications for the use of the 231Pa/230Th ratio as a paleoproductivity proxy, Earth Planet. Sci. Lett., 149(1), 85–100, doi:10.1016/S0012-821X(97)00068-X, 1997.

Yang, H. S., Nozaki, Y., Sakai, H. and Masuda, A.: The distribution of 230Th and 231Pa in the deep-sea surface sediments of the Pacific Ocean, Geochim. Cosmochim. Acta, 50(1), 81–89, doi:10.1016/0016-7037(86)90050-5, 1986.

Yong-Liang Yang, Elderfield, H., Pedersen, T. F. and Ivanovich, M.: Geochemical record of the Panama Basin during the Last Glacial Maximum carbon event shows that the glacial ocean was not suboxic, Geology, 23(12), 1115–1118, doi:10.1130/0091-7613(1995)023<1115:GROTPB>2.3.CO, 1995.

Yong Lao, Anderson, R. F., Broecker, W. S., Trumbore, S. E., Hofmann, H. J. and Wolfli, W.: Transport and burial rates of 10Be and 231Pa in the Pacific Ocean during the Holocene period, Earth Planet. Sci. Lett., 113(1–2), 173–189, doi:10.1016/0012-821X(92)90218-K, 1992.

Yu, E.-F.: Variations in the Particulate Flux of 230Th and 231Pa and Paleoceanographic Applications of the 231Pa/230Th Ratio, WHOI/MIT., 1994.

Yu, E.-F., Francois, R. and Bacon, M. P.: Similar rates of modern and last-glacial ocean thermohaline circulation inferred from radiochemical data, Nature, 379(6567), 689–694, doi:10.1038/379689a0, 1996.

Variable	Symbol	Value	Units
Production of ^{231}Pa from U decay	β^{Pa}	2.33*10^{-3}	dpm m^{-3} y
Production of ^{230}Th from U decay	β^{Th}	2.52*10^{-2}	dpm m^{-3} y
Decay constant of ^{231}Pa	λ^{Pa}	2.13*10^{-5}	yr^{-1}
Decay constant of ^{230}Th	λ^{Th}	9.22*10^{-6}	yr^{-1}
Index for ^{231}Pa and ^{230}Th	i		
Index for particle type	j		
Total isotope activity	A_t		dpm m^{-3}
Dissolved isotope activity	A_d		dpm m^{-3}
Particle associated activity	A_p		dpm m^{-3}
Particle settling velocity	w_s	1000	m yr^{-1}
Particle concentration	C		kg m^{-3}
Density of seawater		1024.5	kg m^{-3}
Ratio between particle concentration and density of seawater	R		

Table 1. List of parameters, abbreviations and values.

	CTRL		EXP_1		EXP_2	
	^{231}Pa	^{230}Th	^{231}Pa	^{230}Th	^{231}Pa	^{230}Th
K_{CaCO_3}	2.5*10^{5}	1.0*10^{7}	5*10^{4}	2*10^{6}	1.25*10^{6}	5*10^{7}
K_{opal}	1.67*10^{6}	5*10^{5}	3.33*10^{5}	1*10^{5}	8.33*10^{6}	2.5*10^{6}
K_{POC}	1.0*10^{7}	1.0*10^{7}	2*10^{6}	2*10^{6}	5*10^{7}	5*10^{7}
T(yr)	118	33	501	143	27	9

Table 2. Partition coefficients for different particle types and residence time for ^{231}Pa and ^{230}Th in different experiments. Partition coefficients used in CTRL follows (Chase et al., 2002; Siddall et al., 2005).

WATER COLUMN ACTIVITY	Holocene core-top $^{231}Pa/^{230}Th$
(Guo et al., 1995)	(Yu, 1994)
(Cochran et al., 1987)	(DeMaster, 1979)
(Nozaki et al., 1987)	(Bacon and Rosholt, 1982)
(Bacon and Anderson, 1982)	(Mangini and Diester-Hass, 1983)
(Bacon et al., 1989)	(Kumar, 1994)
(Huh and Beasley, 1987)	(Yang et al., 1986)
(Rutgers van der Loeff and Berger, 1993)	(Anderson et al., 1983)
(Nozaki et al., 1981)	(Anderson et al., 1994)
(Nozaki and Nakanishi, 1985)	(Ku, 1966)
(Mangini and Key, 1983)	(Ku et al., 1972)

(Nozaki and Horibe, 1983)	(Frank et al., 1994)
(Moore, 1981)	(Shimmield et al., 1986)
(Nozaki and Yamada, 1987)	(Frank, 1996)
(Roy-Barman et al., 1996)	(Yong Lao et al., 1992)
(Nozaki and Yang, 1987)	(Francois et al., 1993)
(Moran et al., 1995)	(Anderson et al., 1990)
(Luo et al., 1995)	(Mangini and Sonntag, 1977)
(Colley et al., 1995)	(Schmitz et al., 1986)
(Scholten et al., 1995)	(Shimmield and Price, 1988)
(Cochran et al., 1995)	(Yong-Liang Yang et al., 1995)
(Vogler et al., 1998)	(Müller and Mangini, 1980)
(Moran et al., 1997)	(Mangini and U., 1987)
(Edmonds et al., 1998)	(Scholten et al., 1995)
(Moran et al., 2001)	(Walter et al., 1997)
(Edmonds et al., 2004)	(Lippold et al., 2011)
(Okubo et al., 2007b)	(Lippold et al., 2012b)
(Coppola et al., 2006)	(Bradtmiller et al., 2007)
(Moran et al., 2002)	(Gherardi et al., 2005)
(Okubo et al., 2004)	(Gutjahr et al., 2008)
(Okubo et al., 2007a)	(Hall et al., 2006)
(Okubo et al., 2012)	(Lippold et al., 2011)
(Robinson et al., 2004)	(Roberts et al., 2014)
(Thomas et al., 2006)	(Bradtmiller et al., 2014)
(Trimble et al., 2004)	(Burckel et al., 2016)
(Venchiarutti et al., 2011)	(Hoffmann et al., 2013)
(Hsieh et al., 2011)	(Jonkers et al., 2015)
(Scholten et al., 2008)	(Negre et al., 2010)
(Luo et al., 2010)	
(Deng et al., 2014)	
(Hayes et al., 2013)	
(Hayes et al., 2015)	

Table 3. References for observations of water column ^{231}Pa and ^{230}Th activity and Holocene core-top $^{231}Pa/^{230}Th$.

Figures:

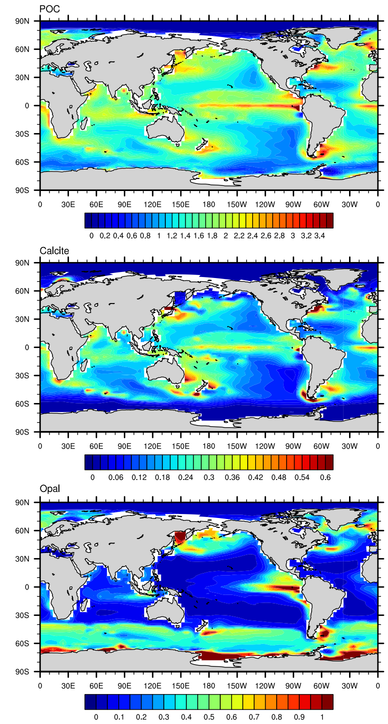

Figure 1. Annual mean particle fluxes in CESM. (a) $CaCO_3$ flux at 105m (mol m^{-2} yr^{-1}). (b) Opal flux at 105m (mol m^{-2} yr^{-1}). (c) POC flux at 105m (mol m^{-2} yr^{-1}).

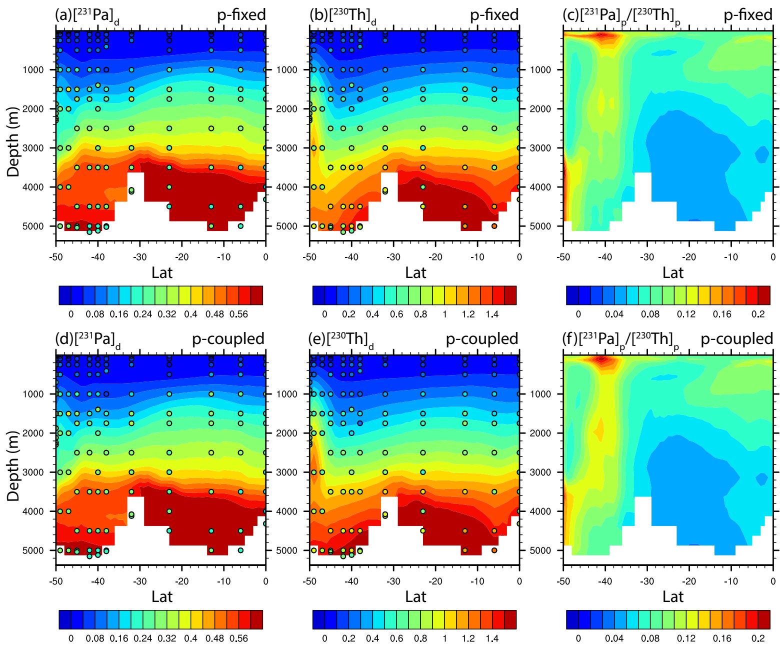

Figure 2. Dissolved ^{231}Pa, dissolved ^{230}Th and particulate $^{231}Pa/^{230}Th$ in CTRL along GEOTRACES transect GA02S (Deng et al., 2014) (the track is indicated in Fig. S4) for both p-fixed and p-coupled ^{231}Pa and ^{230}Th. Observations of dissolved ^{231}Pa and ^{230}Th activity are superimposed using the same colormap.

Deleted: Figure 2. Atlantic zonal mean dissolved and particulate abiotic ^{231}Pa and ^{230}Th in CTRL (unit: dpm/m^3): (a) dissolved ^{231}Pa; (b) dissolved ^{230}Th; (c) particulate ^{231}Pa; (d) particulate ^{230}Th. Scatter plot of global dissolved and particulate ^{231}Pa and ^{230}Th between abiotic and biotic in CTRL: (e) dissolved ^{231}Pa; (f) dissolved ^{230}Th; (g) particulate ^{231}Pa; (h) particulate ^{230}Th. Purple line is the least squared linear regression line and slope is the linear regression coefficient.

Formatted: Not Highlight

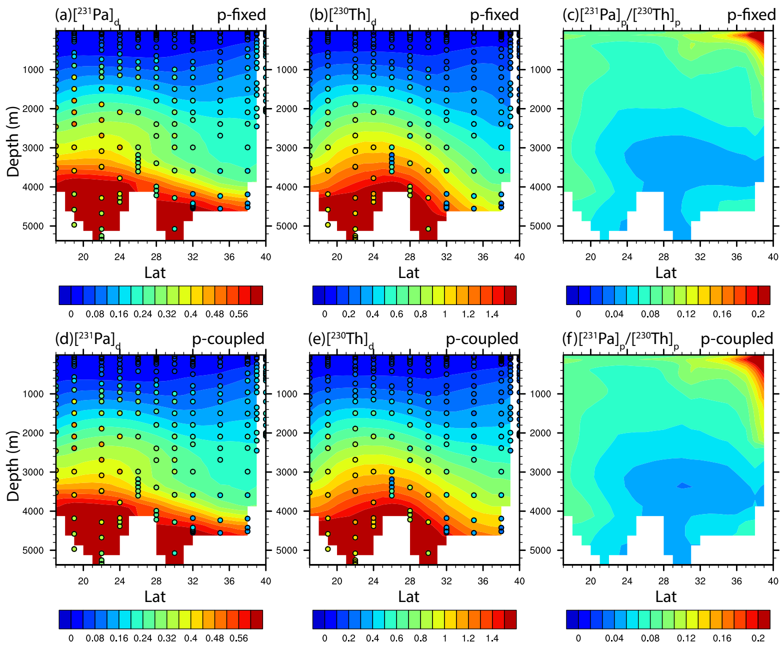

Figure 3. Dissolved ^{231}Pa, dissolved ^{230}Th and particulate ^{231}Pa/^{230}Th in CTRL along GEOTRACES transect GA03 (Hayes et al., 2015) (the track is indicated in Fig. S4) for both p-fixed and p-coupled ^{231}Pa and ^{230}Th. Observations of dissolved ^{231}Pa and ^{230}Th activity are superimposed using the same colormap.

Formatted: Not Highlight

Deleted: ?

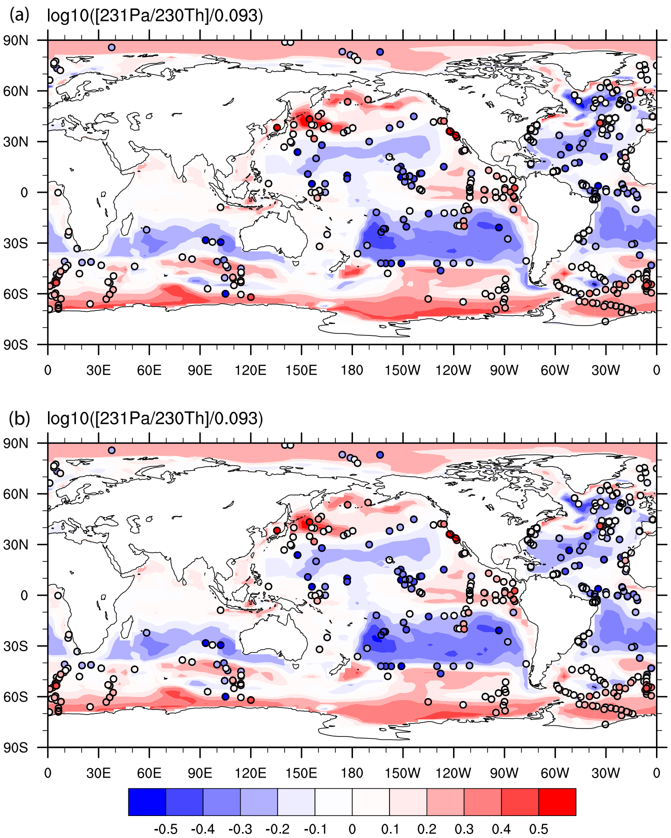

Figure 4. Sediment $^{231}Pa/^{230}Th$ activity ratio in CTRL for both p-fixed (a) and p-coupled version (b). Observations are attached as filled cycles using the same color map. The $^{231}Pa/^{230}Th$ activity ratio is plotted relative to the production ratio of 0.093 on a $\log_{10}$ scale.

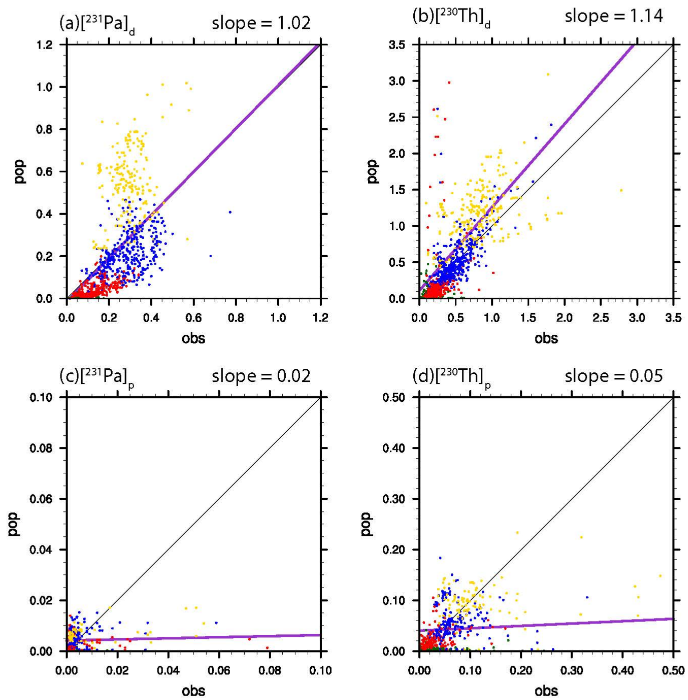

Figure 5. Scatter plot of global dissolved and particulate ^{231}Pa and ^{230}Th between observation and CTRL (p-fixed) (unit: dpm/m^3). (a) dissolved ^{231}Pa; (b) particulate ^{231}Pa; (c) dissolved ^{230}Th; (d) particulate ^{230}Th. Observations in different depth range are indicated by different colors: green for 0-100m; red for 100m-1000m; blue for 1000m-3000m and yellow for deeper than 3000m. Purple line is the least squared linear regression line and slope is the linear regression coefficient.

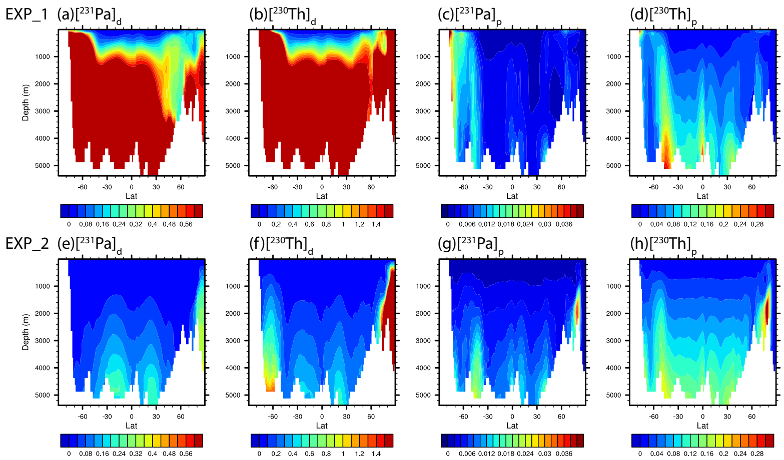

Figure 6. Atlantic zonal mean dissolved and particulate ^{231}Pa and ^{230}Th in EXP_1 and EXP_2 (unit: dpm/m^3). EXP_1: (a) dissolved ^{231}Pa; (b) dissolved ^{230}Th; (c) particulate ^{231}Pa; (d) particulate ^{230}Th. EXP_2: (e) dissolved ^{231}Pa; (f) dissolved ^{230}Th; (g) particulate ^{231}Pa; (h) particulate ^{230}Th.

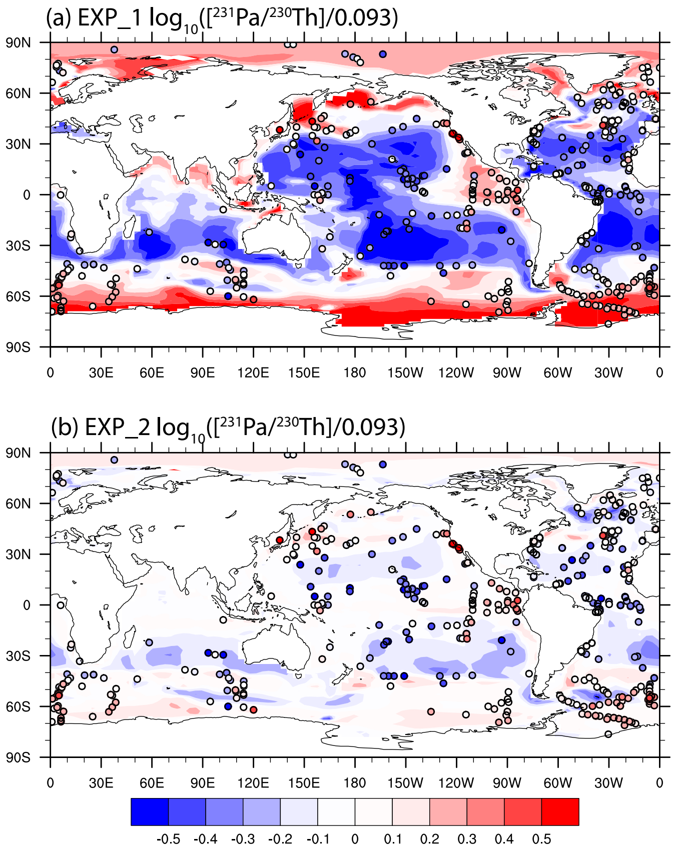

Figure 7. Sediment ^{231}Pa/^{230}Th activity ratio in EXP_1 (a) and EXP_2 (b). Observations are attached as filled cycles using the same color map. The ^{231}Pa/^{230}Th activity ratio is plotted relative to the production ratio of 0.093 on a $\log_{10}$ scale.

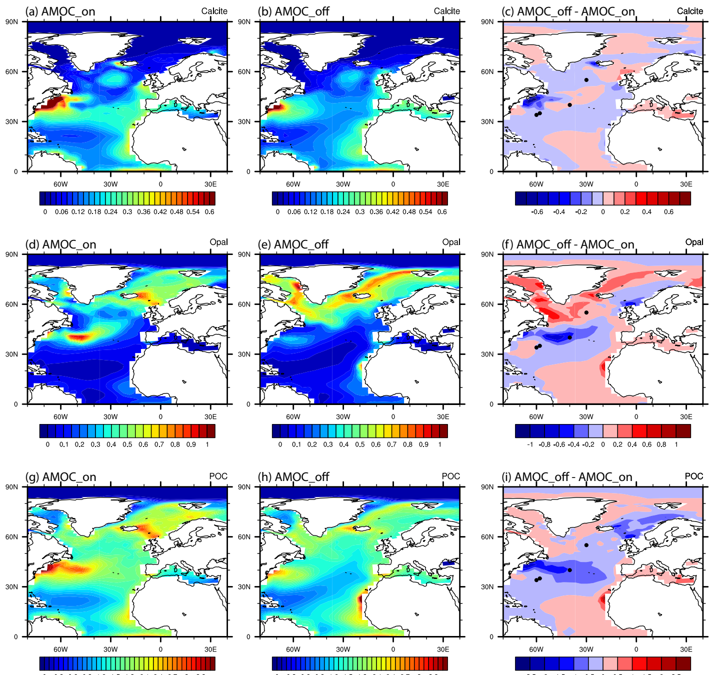

Figure 8. Comparison of particle fluxes between AMOC_on and AMOC_off. $CaCO_3$ flux at 105m (mol m^{-2} yr^{-1}) during AMOC_on (a), AMOC_off (b) and difference between AMOC_off and AMOC_on. (b) Opal flux at 105m (mol m^{-2} yr^{-1}) during AMOC_on (d), AMOC_off (e) and difference between AMOC_off and AMOC_on (f). POC flux at 105m (mol m^{-2} yr^{-1}) during AMOC_on (g), AMOC_off (h) and difference between AMOC_off and AMOC_on (i).

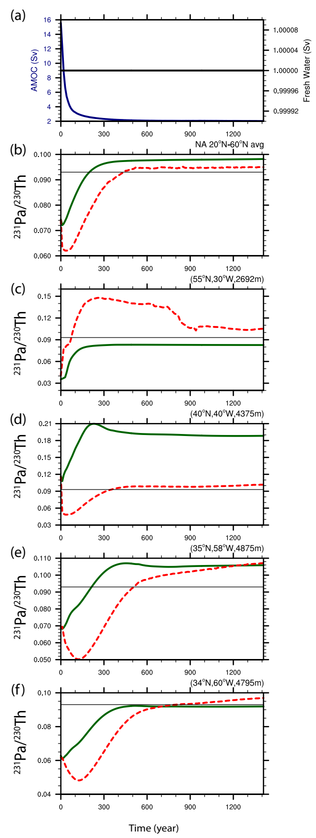

Figure 9. Time evolutions in HOSING. (a) Freshwater forcing (black) and AMOC strength (navy), which is defined as the maximum of the overturning streamfunction below 500m in the North Atlantic. (b) North Atlantic average sediment $^{231}Pa/^{230}Th$ activity ratio from 20°N to 60°N: p-fixed (green) and p-coupled (red). Production ratio of 0.093 is indicated by a solid black line (similar in c, d, e and f). (c) Sediment $^{231}Pa/^{230}Th$ activity ratio at (55°N, 30°W). (d) Sediment $^{231}Pa/^{230}Th$ activity ratio at (40°N, 40°W). (e) Sediment $^{231}Pa/^{230}Th$ activity ratio at (35°N, 58°W). (f) Sediment $^{231}Pa/^{230}Th$ activity ratio at (34°N, 60°W). (e) and (f) are near Bermuda Rise. Locations of each site are shown as dots in Fig. 8b.

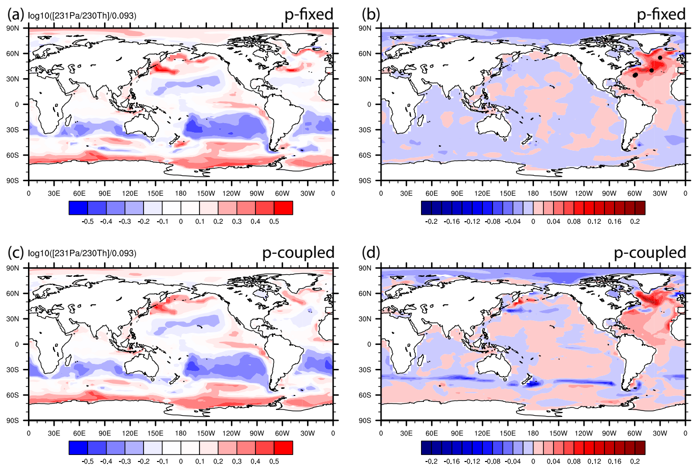

Figure 10. Sediment $^{231}Pa/^{230}Th$ activity ratio during AMOC off state and the difference between AMOC off and CTRL. (a) P-fixed $\log_{10}([^{231}Pa/^{230}Th]/0.093)$ in AMOC_off. (b) Difference of p-fixed sediment $^{231}Pa/^{230}Th$ activity ratio between AMOC_off and AMOC_on. (c) and (d) are similar to (a) and (b) for p-coupled sediment $^{231}Pa/^{230}Th$ activity ratio. Black dots in (b) shows the locations of sites in Fig. 7 from North to South.

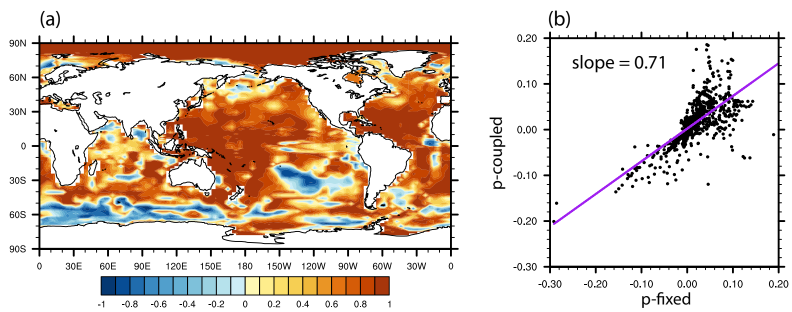

Figure 11. (a) Correlation of p-fixed and p-coupled evolution of sediment $^{231}Pa/^{230}Th$ activity ratio in HOSING. (b) Scatter plot of p-fixed and p-coupled sediment $^{231}Pa/^{230}Th$ activity ratio change from AMOC_on to AMOC_off in the Atlantic and the Southern Ocean (70°W-20°E). Purple line is the least squared linear regression line and slope is the linear regression coefficient.

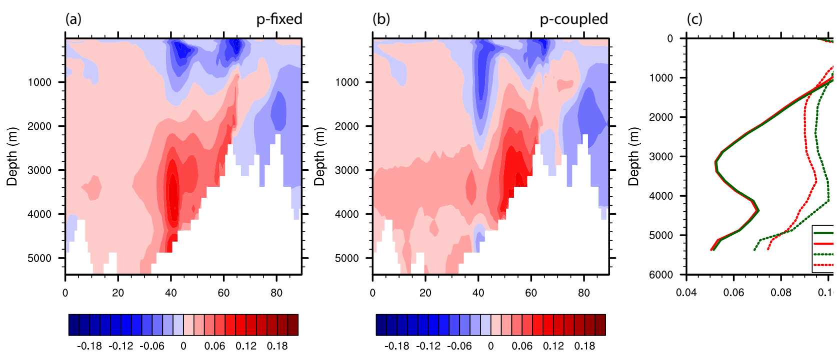

Figure 12. Difference of Atlantic zonal mean particulate $^{231}Pa/^{230}Th$ between AMOC_off and AMOC_on: (a) p-fixed and (b) p-coupled. (c) North Atlantic (20°N-60°N) average profile during AMOC_on (solid) and AMOC_off (dash) for p-fixed (green) and p-coupled (red) particulate $^{231}Pa/^{230}Th$.

1742
1743
1744
1745

Page 17: [1] Deleted	Microsoft Office User	7/19/17 12:57:00 PM

Two forms of ^{231}Pa and ^{230}Th are implemented in POP2: abiotic and biotic. Abiotic ^{231}Pa and ^{230}Th use particle fluxes prescribed as annual mean particle fluxes from the CESM marine ecosystem module under present day climate forcing (Fig.1). Biotic ^{231}Pa and ^{230}Th use particle fluxes computed simultaneously from the marine ecosystem module. Abiotic and biotic ^{231}Pa and ^{230}Th can be turned on at the case build time and the biotic ^{231}Pa and ^{230}Th requires the ecosystem module turned on at the same time.

The implementation of ^{231}Pa and ^{230}Th is based on Siddall et al., (2005) (Eq.(3)). ^{231}Pa and ^{230}Th are produced from the α decay of ^{235}U and ^{234}U uniformly everywhere at constant rate β^i (β^{Pa} = 2.33*10^{-3} dpm m^{-3} yr^{-1}, β^{Th} = 2.52*10^{-2} dpm m^{-3} yr^{-1}). ^{231}Pa and ^{230}Th are subjective to radioactive decay with the decay constant of λ^i (λ^{Pa} = 2.13*10^{-5} yr^{-1}, λ^{Th} = 9.22*10^{-6} yr^{-1}). In addition to ocean transport, which includes advection, convection, and diffusion, another

Page 19: [2] Deleted	Microsoft Office User	7/18/17 5:32:00 PM

$$A_t^i = A_d^i + A_p^i \qquad (1)$$

$$K_j^i = \frac{A_{j,p}^i}{A_{j,d}^i C_j} \qquad (2)$$

Page 19: [3] Deleted	Microsoft Office User	7/19/17 1:02:00 PM

where

Page 19: [4] Deleted	Microsoft Office User	7/18/17 5:52:00 PM

.

$$A_p^i = A_t^i \cdot (1 - \frac{1}{1 + K_{POC}^i \cdot R_{POC} + K_{CaCO_3}^i \cdot R_{CaCO_3} + K_{opal}^i \cdot R_{opal} + K_{dust}^i \cdot R_{dust}}) \qquad ($$

Page 25: [5] Deleted	Microsoft Office User	7/24/17 4:47:00 PM

With the AMOC collapsing, the $^{231}Pa/^{230}Th$ ratio tends to increase over most of the North Atlantic, consistent with paleo proxy evidence there. In HOSING, after applying extra freshwater to the North Atlantic, AMOC strength quickly decreases to a minimum of 2 Sv at around year 300 (AMOC_off)(Fig. 7a). During the AMOC_off state, compared with CTRL of active AMOC (AMOC_on), both abiotic and biotic sediment $^{231}Pa/^{230}Th$ ratio shows an overall increase in the North Atlantic and a decrease in the South Atlantic (Fig. 8b and d) because of the reduced southward transport of ^{231}Pa from the North Atlantic by AMOC. In most area of the Atlantic, the evolution of abiotic and biotic sediment $^{231}Pa/^{230}Th$ activity ratio in HOSING are highly correlated (Fig. 9a). The change of sediment $^{231}Pa/^{230}Th$ ratio from AMOC_on to AMOC_off are similar in abotic and biotic version (Fig.9b). The correlation between abiotic and biotic sediment $^{231}Pa/^{230}Th$ ratio change is 0.72 (1455points) and the linear regression coefficient is 0.71 (R^2 = 0.52). This suggests that abiotic sediment $^{231}Pa/^{230}Th$ activity ratio can capture the major feature of biotic $^{231}Pa/^{230}Th$ activity ratio in our model and also circulation effect on sediment $^{231}Pa/^{230}Th$ activity ratio is more dominant than the biological effect in HOSING. The pattern of abiotic (Fig.8a) sediment $^{231}Pa/^{230}Th$ ratio in the Atlantic in AMOC_off state is similar to the opal distribution (Fig.1b) because, without active circulation, sediment $^{231}Pa/^{230}Th$ ratio is more controlled by particle flux effect, which is similar to the case in the Pacific in CTRL. The overall increase of sediment $^{231}Pa/^{230}Th$ ratio in the North Atlantic in response to AMOC collapse can be seen more clearly in the time evolution of the sediment $^{231}Pa/^{230}Th$ ratio averaged from 20°N to 60°N in the North Atlantic in both the abiotic and biotic $^{231}Pa/^{230}Th$ (Fig.7b). Quantitatively, the $^{231}Pa/^{230}Th$ increases from 0.074 (0.074) in AMOC_on to 0.098 (0.095) in AMOC_off in the abiotic (biotic) version (Fig. 7b). Both abiotic and biotic version show average sediment $^{231}Pa/^{230}Th$ ratio in the North Atlantic near the production ratio of 0.093. This increase of $^{231}Pa/^{230}Th$ in both abiotic and biotic versions is also seen in the subtropical North Atlantic from the two sites near Bermuda Rise (Fig. 7e and f), which is, of comparable magnitude with the change from LGM to HS1 in reconstructions there (McManus et al., 2004). It is further noted that our abiotic sediment $^{231}Pa/^{230}Th$ ratio in HOSING behaves similarly to that in Siddall et al., (2007).

In spite of large scale patterns of sediment $^{231}Pa/^{230}Th$ ratio response, the magnitude of the change between AMOC_on and AMOC_off varies with location in both abiotic and biotic version because of the distribution of particle flux (Fig.7 and 8). Take the abiotic version as an example, the maximum increase in sediment $^{231}Pa/^{230}Th$ ratio occurs near 40°N western Atlantic, where the opal production in our model is maximum (Fig. 1b). The sediment $^{231}Pa/^{230}Th$ ratio in this region in AMOC_on is larger than production ratio of 0.093 because particle flux effect due to the opal maximum provides extra ^{231}Pa to this region, which overwhelms the active ocean circulation transporting ^{231}Pa southward outside this region. Therefore, sediment ^{231}Pa/^{230}Th ratio in this region gets even larger (e.g. Fig. 7d). In AMOC_off, without active ocean circulation, the particle flux effect becomes more prominent because less ^{231}Pa is transported out of the North Atlantic.

Page 38: [6] Deleted **Microsoft Office User** **7/19/17 2:10:00 PM**

K_{dust}	0	0	0	0	0	0